NASA CR-134651

SINGLE CRYSTAL MEMBRANES

by R. W. Stormont and A. Morrison

TYCO LABORATORIES, INC.

Prepared for

NATIONAL AERONAUTICS AND SPACE ADMINISTRATION

NASA Lewis Research Center
Contract No. NAS3-17346

1. Report No.	2. Government Accession No.	3. Recipient's Catalog No.
NASA CR-134651		

4. Title and Subtitle	5. Report Date
SINGLE CRYSTAL MEMBRANES	April 1974
	6. Performing Organization Code

7. Author(s)	8. Performing Organization Report No.
R. Stormont A. Morrison	C-362
	10. Work Unit No.

9. Performing Organization Name and Address	11. Contract or Grant No.
Tyco Laboratories, Inc. 16 Hickory Drive Waltham, Massachusetts 02154	NAS3-17346
	13. Type of Report and Period Covered
12. Sponsoring Agency Name and Address	Contractor Report
NASA-Lewis	14. Sponsoring Agency Code

15. Supplementary Notes

Project Manager, Albert C. Antoine

16. Abstract

Single crystal a- and c-axis tubes and ribbons of sodium beta-alumina and sodium magnesium beta-alumina were grown from sodium oxide rich melts. Additional experiments grew ribbon crystals containing sodium magnesium β, β'', β''', and β'''' aluminas.

The crystal growth of beta-alumina is made complicated by its high sodium vapor pressure, peritectic decomposition, and highly reactive melt. However, the use of a high pressure [2.0 MN/m^2 (300 psi)] crystal growth chamber, sodium oxide rich melts, and iridium for all surfaces in contact with the melt were combined with the edge-defined, film-fed growth (EFG) technique to grow the single crystal beta-alumina tubes and ribbons. The crystals were characterized using metallographic and X-ray diffraction techniques, and wet chemical analysis was used to determine the sodium, magnesium, and aluminum content of the grown crystals.

17. Key Words (Suggested by Author(s))	18. Distribution Statement
High Pressure Furnace Beta-Alumina Single Crystal Membranes Batteries EFG Crystal Growth	Unclassified-unlimited

19. Security Classif. (of this report)	20. Security Classif. (of this page)	21. No. of Pages	22. Price*
UNCLASSIFIED	UNCLASSIFIED	52	

* For sale by the National Technical Information Service, Springfield, Virginia 22151

ABSTRACT

Single crystal a- and c-axis tubes and ribbons of sodium beta-alumina and sodium magnesium beta-alumina were grown from sodium oxide rich melts. Additional experiments grew ribbon crystals containing sodium magnesium β, β'', β''', and β'''' aluminas.

The crystal growth of beta-alumina is made complicated by its high sodium vapor pressure, peritectic decomposition, and highly reactive melt. However, the use of a high pressure [2.0 MN/m^2 (300 psi)] crystal growth chamber, sodium oxide rich melts, and iridium for all surfaces in contact with the melt were combined with the edge-defined, film-fed growth (EFG) technique to grow the single crystal beta-alumina tubes and ribbons. The crystals were characterized using metallographic and X-ray diffraction techniques, and wet chemical analysis was used to determine the sodium, magnesium, and aluminum content of the grown crystals.

Table of Contents

List of Illustrations

List of Tables

I. SUMMARY

This program was an extension of work begun under Contract Nos. NAS3-14410 and NAS3-15686. Those programs had as their objective the development of single crystal membranes of solid ionic conductors, especially β-alumina, which have potential application in high energy density batteries operating at moderate to ambient temperatures. Using the Tyco-developed EFG melt growth techniques, iridium system components and a high pressure (2 MN/m^2) furnace chamber, the programs demonstrated the growth of single phase single crystal β-alumina tubes of the desired orientations. However, the crystals grown under those programs had a tendency to crack along the cleavage plane during growth and very slow growth rates (2 mm/hr) were required to obtain transparent single crystals free of phase inclusions.

The specific objectives of this program were to determine the optimum growth conditions of β-alumina, to obtain non-coated transparent single crystal tubes and ribbons, to eliminate or reduce thermal stresses which lead to cracks, and to grow β-alumina tubes with varying amounts of Na_2O, MgO, and Al_2O_3 to enhance ionic conductivity and mechanical strength.

Single crystal single phase tubes and ribbons of beta-alumina containing Na_2O and Na_2O plus MgO were grown as verified by Debye-Scherrer X-ray powder patterns, Laué back reflection X-ray photographs, and chemical analysis. Magnesium oxide stabilized ribbons which were found to contain β, β'', β''', and β'''' were also grown.

Although several uncracked tube crystals were grown, the majority of the crystals were cracked, and depending on the afterheater configuration, they were all invariably coated with either an Al_2O_3 or a Na_2O 'skin'. The crystals also tended to become multi-grained and contained second phase inclusions when grown at speeds greater than 6 mm/hr.

II. INTRODUCTION

A recent development of great technological potential is the concept of a high energy density battery utilizing a solid, super ionic conductor as the electrolyte.[1] One of the best super ionic conductors for such application is β-alumina (nominally: $Na_2O \cdot 11\ Al_2O_3$)[2]. Crystals of this compound have very low electronic conductivity, negligible ionic conductivity in the direction of the hexagonal crystalline c-axis, and very high sodium ion conductivity in directions normal to the c-axis.[2-5] Obvious advantages will accrue from the use of single crystalline membranes of the correct orientation. Even if the polycrystalline aggregates are of preferred orientation, the presence of grain boundaries provides additional problems, since intergranular processes may occur, resulting in failure of the conducting path. It is possible that lower operating temperatures may result from the use of single crystal materials. Thus, the establishment of a method for the growth of single crystal β-alumina is of considerable interest.

To date, electrochemical studies and prototype batteries have utilized only small single crystal wafers or sintered polycrystalline tubes of β-alumina. Under two preceding contracts,[6,7] Tyco developed techniques for producing c-axis tubes of β-alumina. Clearly, this constituted a major step toward the realization of high energy density batteries such as conceived by Weber and Kummer.[1]

This program was an effort to improve the quality of the crystals to the point where useful material could be regularly produced and the effects of composition and growth conditions on ionic conductivity could be measured. In the following sections we describe the program aimed at optimizing and defining the conditions for growth of sound, highly conducting, tubular and ribbon shaped crystals of β-alumina. Work under a previous contract[6] had established that MgO can be substituted in the β-alumina

crystals during growth. MgO stabilized β''-alumina (approximate stoichiometry 10.0 MgO 12.5 $Na_2O \cdot$ 77.5 Al_2O_3) was also grown under this program. This phase is also a super ionic conductor with a structure similar to that of β-alumina and with even higher sodium ion conductivity.

III. APPARATUS AND BASIC EXPERIMENTAL PROCEDURES

A. Apparatus

Because of the high loss of sodium by volatilization at the growth temperature under atmospheric conditions,[7] a furnace chamber (designed and built at Tyco) was used which would allow the growth of crystals under inert gas pressures up to $2MN/m^2$ (300 psi). The addition of excess soda to the melt together with the use of the high pressure furnace was necessary for the successful growth of single crystal beta-alumina.[6, 13]

The furnace is shown schematically in Fig. 1 and was used for the growth of all beta-alumina tube and ribbon crystals. The pressure vessel consists of a 30 cm diameter by approximately 60 cm high 304 S/S split chamber, designed for 2 MN/cm^2 at 541 K. The chamber is water jacketed and mounted on a suitable stand with a hand-operated hydraulic mechanism to raise and lower the bottom section approximately 30 cm. The lower section swings away in the lowered position for accessibility.

The furnace was designed to allow the growth of crystal tubes up to 20 cm long and includes the following features:

1. On top is mounted a linear motion device suitable for withdrawal of crystals at rates of up to 2.5 cm/min.*
2. 10 cm port for RF power feedthroughs.
3. 5 cm inner dia sight ports (2) at 20° incline from horizontal.

---

*A.D. Little Co., Cambridge, Massachusetts

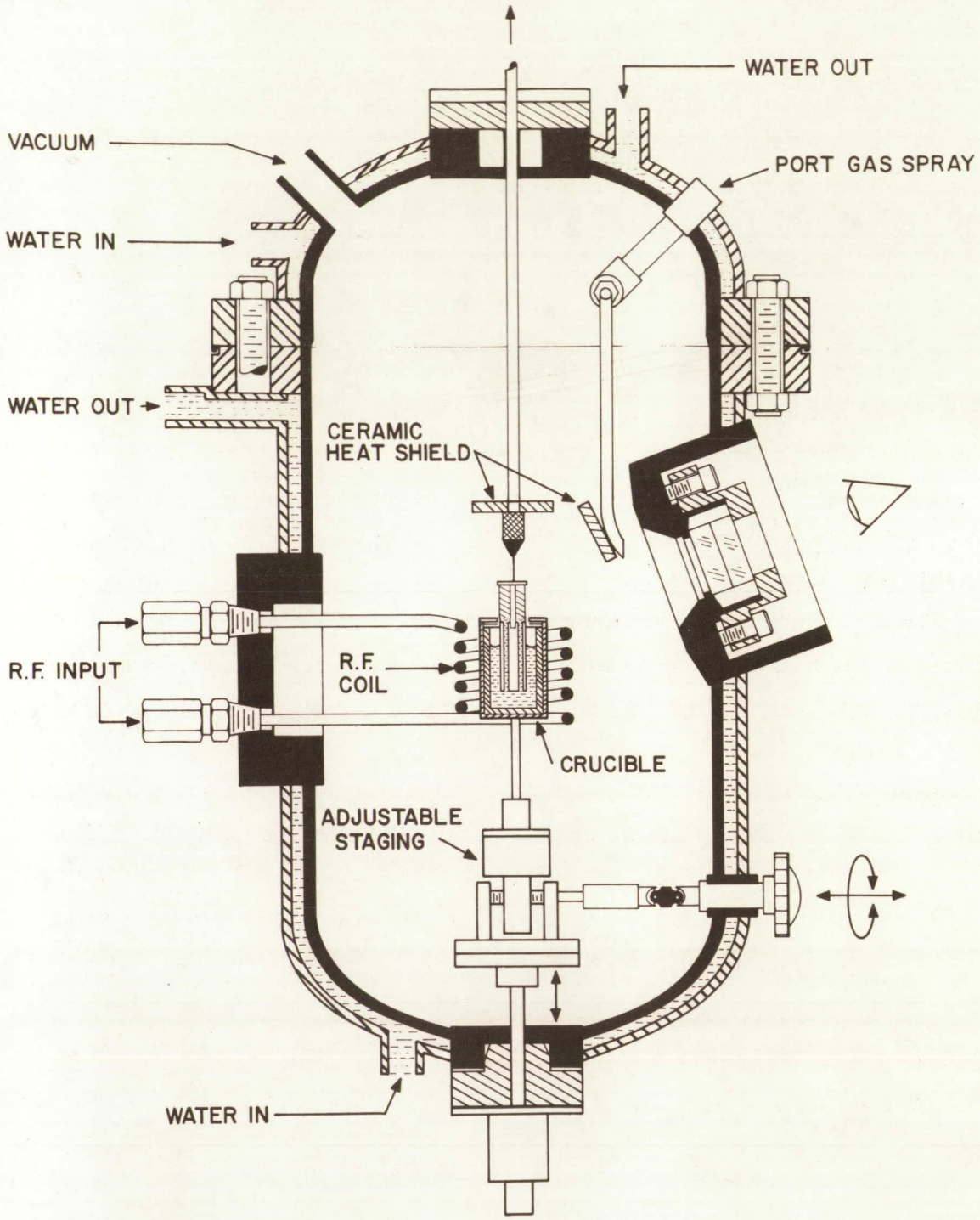

Fig. 1. Schematic of high pressure crystal growth chamber

4. 2.5 cm vacuum port.

5. Feedthroughs complete with manually-controlled x-y and vertical motion device allowing precise location of crucible (x-y motion is ± 6 mm and the vertical motions ± 13 mm).

6. Various 1.3 to 2.5 cm ports required for evacuation; introduction of inert gas and measurement of gas pressure.

The entire high pressure crystal growing furnace is shown photographed in Fig. 2.

In this system, first a 450 kHz 20 kW rf generator and then a 20 kW, 10 kHz, motor generator was used to raise the crucible containing the melt to the necessary growth temperature either by susception directly to the crucible or to a susceptor surrounding it. The advantages of the motor generator over the higher frequency rf set are the low voltage on the coil during use which reduces the tendency for arcing and heating of the power feedthroughs.[7, 13, 14]

B. Starting Materials

There is a continuing uncertainty with regard to the exact composition of beta-alumina. The material commonly obtainable in such form and known as carborundum Monofrax H beta-alumina is $Na_2O \cdot 11\ Al_2O_3$ (8.34 mole % Na_2O). This material was used as the starting charge for many of the growth experiments. Weber and Venero[15] reported the composition of beta-alumina as being 10 mole % Na_2O with an incongruent melting point at 2240 ± 6°K (Fig. 3). Harata[16] reported that Monofrax H cast bricks contain small amounts of alpha-alumina as a second phase and that single phase β-alumina has the composition range 10.9 to 13.7 mole % Na_2O. Considerable MgO can also be incorporated in the β-alumina phase (up to the composition 6.5 MgO 10.5 $Na_2O \cdot 83\ Al_2O_3$).[20] Still higher MgO content (10. mole %) changes the lattice to the β''-alumina structure (Fig. 4).

Monofrax H beta-alumina was used as the starting material in most beta-alumina growth experiments, with excess Na_2O added to vary the composition from 8.4% to 20% Na_2O, with MgO being added up to 10.0 mole % for specific growth runs. Typically, mixtures of Na_2CO_3,* MgO,** and Monofrax H*** beta-alumina were weighed into 2 to 9 g charges and placed in the iridium crucible and melted under 1.4 MN/m^2.

*United Mineral Co. 99.999%.
**Fischer Scientific Reagent Grade
***Carborundum Co., Falconer, N.Y.

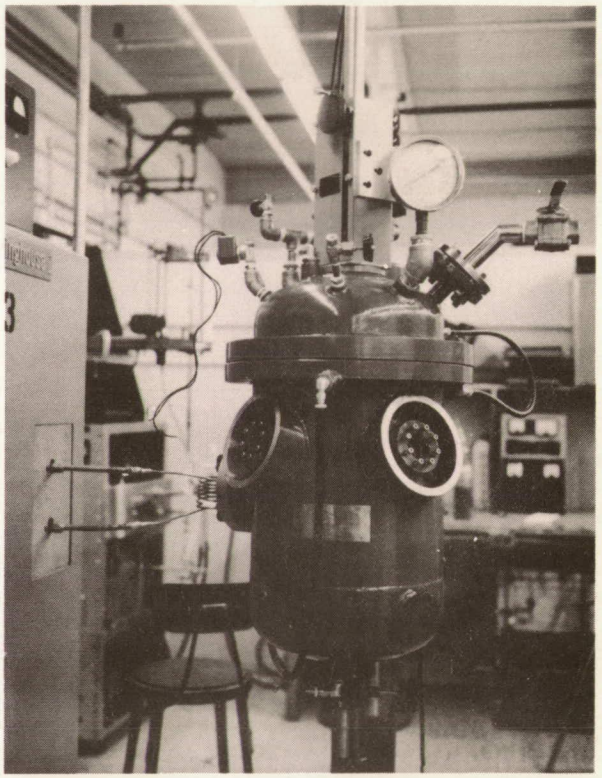

Fig. 2. High pressure crystal growth furnace

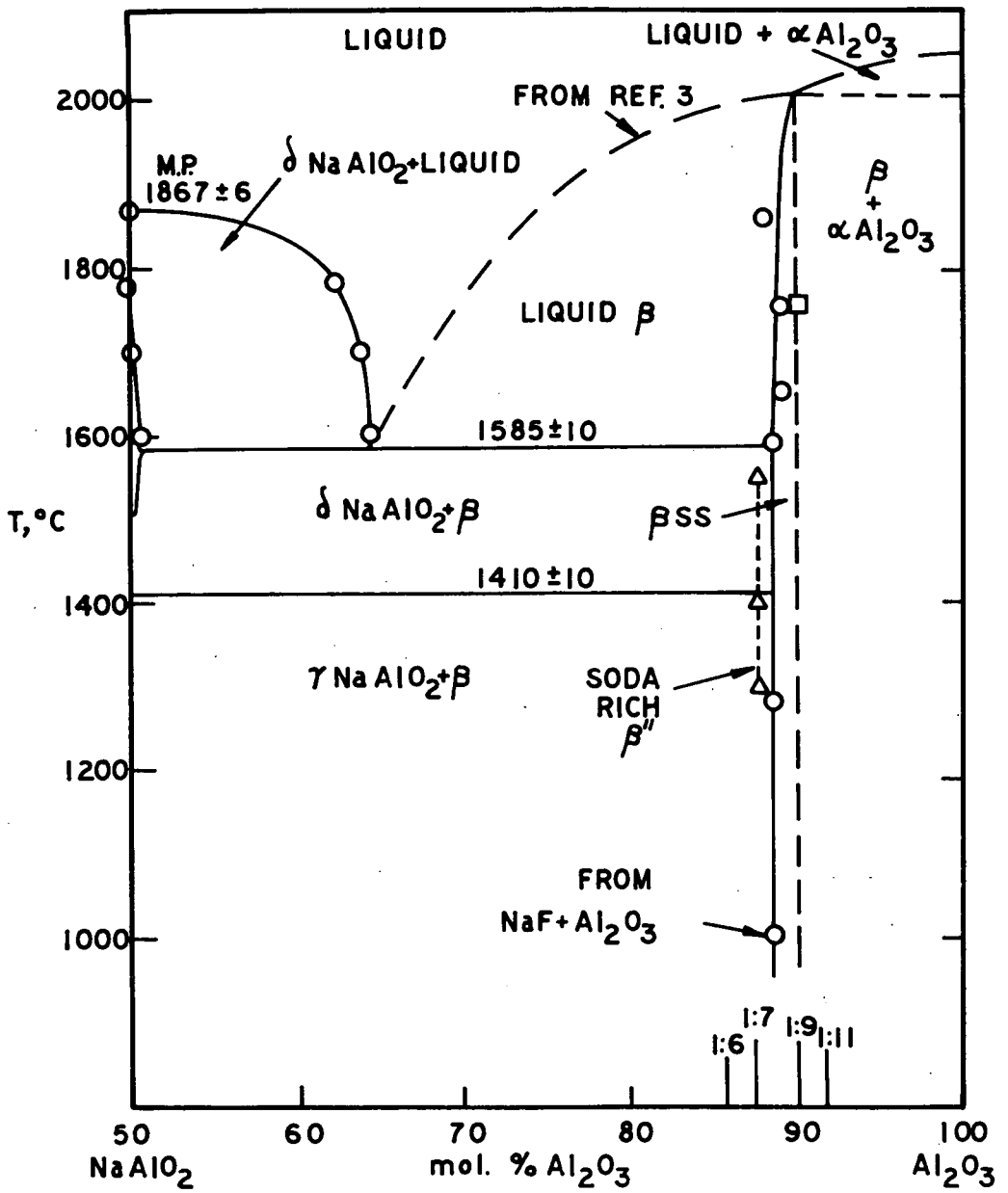

Fig. 3. Section of the Na_2O-Al_2O_3 pseudobinary diagram containing β and β "-alumina. Taken from reference 15.

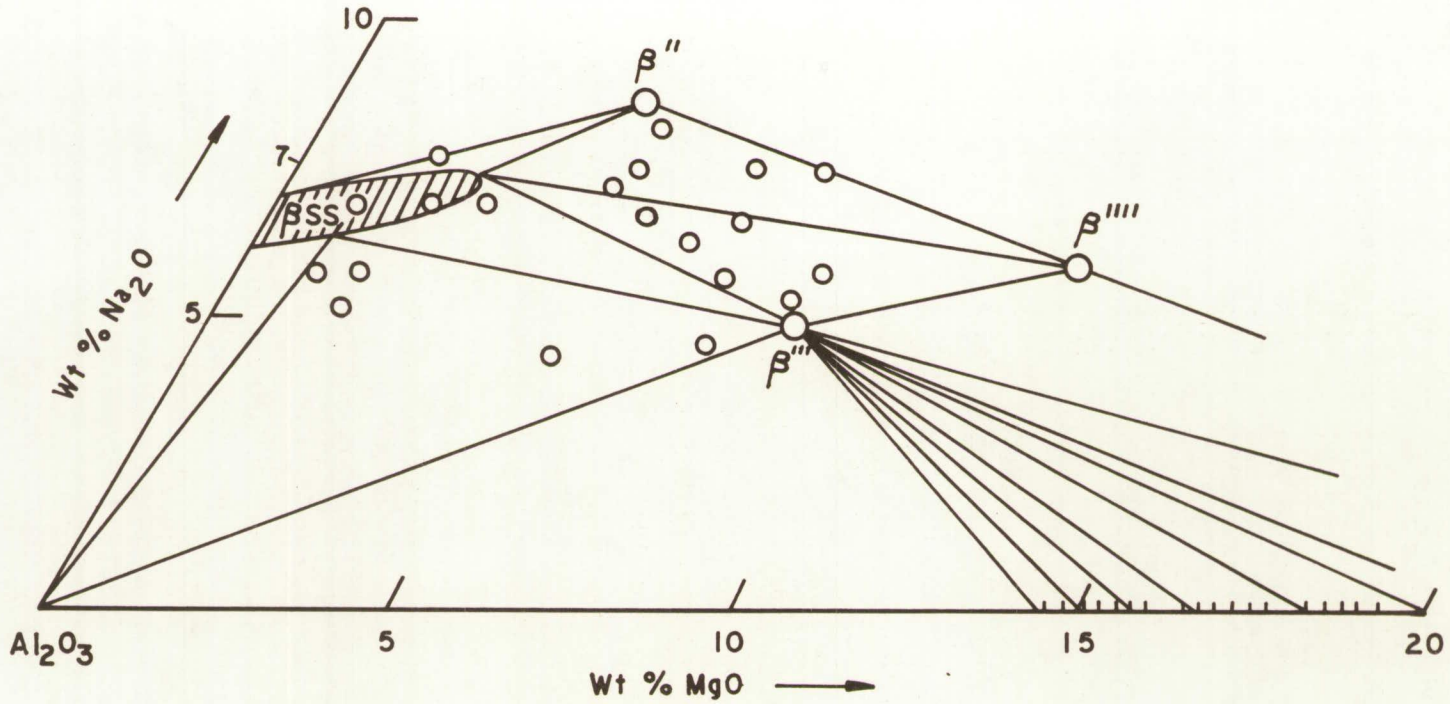

Fig. 4. Section of ternary system Na_2O-Al_2O_3-MgO at 1700°C. Taken from reference 20.

A sample of Monofrax H used for starting material was submitted to semi-quantitative spectrographic analysis and the results are listed in Table I, together with the analysis of a 100% beta-alumina tube crystal grown from a melt of Monofrax H containing 3 mole % excess Na_2O ($\sim Na_2O$)$_{0.13}$ (Al_2O_3)$_{0.87}$.

C. Growth Process

Tubes and ribbons were grown from beta-alumina melts using the Tyco developed melt growth technique, "edge-defined, film-fed growth" (EFG) [17, 18] at speeds from 1 to 250 mm/hr. This technique is a modified pulling technique where the crystal grows remote from the bulk of the melt and crystal cross-section shapes can be arbitrarily chosen.

A crucible and die setup capable of growing sodium beta-alumina tubes was assembled from iridium components. The die used allowed the growth of tubes 5 mm outer dia × 3.5 mm inner dia. All sodium beta-alumina tube growth experiments were made using this size iridium tube setup (see Fig. 5).

All the growth experiments were made in argon at 1.1 to 1.6 MN/m^2 inside a water cooled pressure chamber using a 20 kW, 450 kHz rf or 20 kW, 10 kC, motor generator set as the power supply (see Figs. 1 and 2 and Table II). The 19 mm outer dia × 19 mm high × 0.5 mm wall iridium crucible, containing the sodium beta-alumina charge material and the iridium tube die were both placed inside a 2.5 cm outer dia. Mo crucible with W liner and suscepted to directly. Manual temperature control was by a multiturn potentiometer arrangement of the manufacturer's design.

Only iridium crucible and die components were used in contact with the beta-alumina melts. The seeds used to initiate growth were pieces of Monofrax H single crystals orientated in either the a- or c-axis direction (Tables II and III).

The crystals grown were examined using optical microscopy in transmitted and reflected light. The composition and occurrence of second phase in the crystals grown were determined using standard Debye-Scherrer examination of powdered samples and comparing the pattern and line intensities with standard films and literature values. Laué X-ray back reflection photography was used to study the crystallinity of the samples grown. Wet chemical analysis was used to determine the Na, Mg, and Al content of the grown crystals.

Sample: 1 = (Monofrax H) Beta-Alumina $Na_2O.11\ Al_2O_3$
2 = H.P.-19AF (top)
3 = H.P.-19AF (bottom)

Instrumentation: 3.4 Meter Mark IV Spectrograph

	1	2	3		1	2	3		1	2	3		1	2	3
Li	ND	ND	ND	Zn	ND	ND	ND	Sb	ND	ND	ND	Lu	ND	ND	ND
Be	ND	ND	ND	Ga	T	300	500	Te	ND	ND	ND	Hf	ND	ND	ND
B	ND	1	3	Ge	ND	ND	ND	Cs	ND	ND	ND	Ta	ND	ND	ND
Na	M	M-H	M-H	As	ND	ND	ND	Ba	ND	ND	ND	W	ND	ND	ND
MG	VFT FT	0.5%	0.5%	Rb	ND	ND	ND	La				Re	ND	ND	ND
Al	H	H	H	Sr	ND	ND	ND	Ce				Os	ND	ND	ND
Si	L-M	1%	M	Y				Pr				Ir	ND	ND	ND
K	ND	ND	ND	Zr	ND	ND	ND	Nd				Pt	ND	ND	ND
Ca	VFT	100	500	Nb	ND	ND	ND	Sm				Au	ND	ND	ND
Ti	FT	ND	ND	Mo	ND	75	25	Eu				Hg	ND	ND	ND
V	ND	ND	ND	Ru	ND	ND	ND	Gd				Ti	ND	ND	ND
Cr	VFT	0.25	0.25	Rh	ND	ND	ND	Tb				Pb	ND	10	10
Mn	FT	5	10	Pd	ND	ND	ND	Dy				Bi	ND	ND	ND
Fe	T-L	0.1%	0.2%	Ag	ND	ND	0.1	Ao				Tb			
CO	ND	25		Cd	ND	ND	ND	Er				U			
Ni	ND	10	10	In	ND	ND	ND	Tm				P	ND	ND	ND
Cu	VFT	1	2	Sn	ND	ND	ND	Yb				Se			

*Analysis performed by Jarrell-Ash Division, Fisher Scientific Company
Results in ppm except where % is indicated.

KEY: ND - Not Detected
VVFT < 0.0001%
VFT 0.0001% - 0.001%
FT 0.001% - 0.01%
T 0.01% - 0.1%
L 0.1% -1%
M 1% - 10%
H > 10%

Table I. Semi-Quantitative Spectrographic Analysis

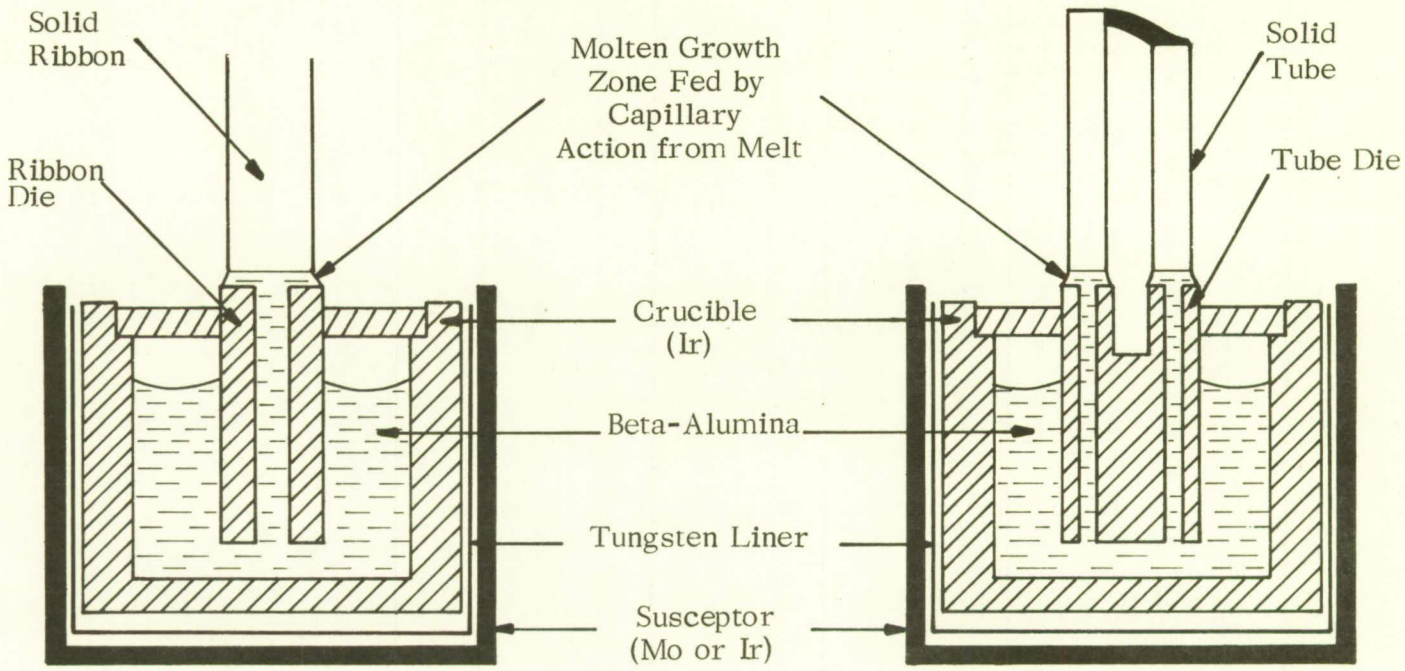

Fig. 5a. Schematic diagram showing crucible and die setup used for growth of ribbons

Fig. 5b. Schematic diagram showing crucible and die setup used for growth of tubes

Table II. Tube Growth

Run No.	Afterheater Setup	Melt Composition (mole % Na_2O)	Charge Size (grams)	Gas Pressure (MN/m^2)	Growth Speed (mm/hr)	Seed Orientation	Comments	Results
H.P.-1AF*	2 cm dia × 5 cm long Indium tube	15.0	7.5	1.2	2 - 12	c-axis	Five starts, seeds broke four times	Tube crystal, 5.25 cm long, 100% β with α skin patches, not single, no deposit from growth.
H.P.-2AF*	Mo tube, 2.5 cm O.D. × 1.9 cm I.D. × 3.2 cm long	Same charge	Same charge 2n run	1.4	2 - 4.5	c-axis	Crystal clear as it grew just above die ~1 mm, then became cloudy	Seed broke, not complete tube 1.9 cm long, 100% β-c-axis, with α skin at top, bottom Na_2O rich.
H.P.-3AF*	Same	Same charge	Same charge	1.2 - 1.4	2 - 12	c-axis	Piece of full tube as seed, sapphire tube around die	Tube crystal 3.7 cm long, 100% β, 3/4 of circumference c-axis, rest a-axis with α-skin.
H.P.-4AF*	Same	Same charge	Same charge	1.2 - 1.4	2	c-axis	No shield on top after heater, coil lower, seed broke	Piece of tube crystal 4.7 mm long not complete tube, $\alpha + \beta$ poly with α skin
H.P.-5AF*	Same	Same charge	Same charge	1.4	No growth	-	No growth, held piece of tube above die, then placed on die	Converted piece of β tube to α-Al_2O_3 when held on die for 1.5 hrs.
H.P.-6AF*	Same	Same charge	Same charge	1.4	No growth	-	Same as above but lower afterheater temperature	Converted piece of single crystal β tube to α-Al_2O_3 3 hrs.
H.P.-7AF*	No afterheater, coil even with top of susceptor	18.0	6	1.4	2 - 6	c-axis	Seed almost complete β-tube piece	Tube crystal 4.1 cm long, 100% β, c-axis single, deposit on tube from growth.
H.P.-8AF*	No afterheater, coil even with top of susceptor	Same charge	Same charge	1.4	2 - 7	a-axis	Seeded on two sides, difficulty spreading to complete tube	Tube crystal 4.1 cm long, 100% β, a-axis single crystal, very clear at top then less clear towards bottom
H.P.-9AF*	No top shield on susceptor	Same charge	Same charge	1.4	2 - 6	c-axis	Large meniscus during growth, no deposit 1 cm up from bottom, then coated	Tube crystal 4.5 cm long, first 6 mm c-axis then shifts to a-axis 100% β-alumina.
H.P.-10AF*	Ceramic insulator, susceptor to Ir crucible	Same charge	Same charge	1.4 - 1.7	2 - 9	c-axis	Seed broke during seeding, lifted up with α-filament	5 cm long tube crystal, 3/4 dia c-axis, rest a-axis, 100% β.
H.P.-11AF	Ceramic insulator, susceptor to Ir crucible	Same charge	Same charge	1.0	2 - 3	c-axis	Developed horizontal cracks as it grew	Tube ~6.5 cm long, not single, top 98% β-bottom 2% β

Table IL (continued)

Run No.	Afterheater Setup	Melt Composition (mole % Na_2O)	Charge Size (grams)	Gas Pressure (MN/m^2)	Growth Speed (mm/hr)	Seed Orientation	Comments	Results
H.P.-12AF†	Ceramic setup Mo shield in coil	11.0	2	1.0	2 - 9	c-axis	Two starts, seed broke first time	X-tal froze to die, 1.5 cm long tube 80% β-not single
H.P.-13AF†	Mo susceptor, low in coil	11.0	2	1.0	2 - 27	c-axis	New crucible + tube die - pulled crucible empty	Tube crystal 6.3 cm long, poly, 70% β - 30% α, light blue color
H.P.-14AF†	Mo susceptor, low in coil	11.0	1.5	0.7	2 - 27	c-axis	Seed broke, froze, re-dipped, cracked above top shield	5.0 cm tube crystal, light blue color, poly, 80% β - 20% α-alumina
H.P.-15AF†	Lower in coil	13.0	1.5	1.0	2 - 9	c-axis	Difficulty spreading, re-dipped twice	4.8 cm tube crystal, poly 99 - 100% α-Al_2O_3
H.P.-16AF†	Lower in coil	13.0	2	1.0	2 - 9	c-axis	Seed broke twice, had to abort run early	6 mm long tube, bluish in color, poly, α+β -alumina
H.P.-17AF†	Same	13.0 + 2 w/o MgO	2	1.0	2 - 27	c-axis	Grew to empty crucible (new crucible)	6.0 cm long tube crystal, poly, α β -alumina
H.P.-18AF†	Same	13.0 + 2 w/o MgO	1.5	1.0	2 - 27	c-axis	Grew to empty old crucible	5.0 cm long tube, poly tube, α - β alumina
H.P.-19AF†	Mo susceptor, no after-heater	13.0	6	1.0	1 - 27	c-axis	Seed broke on dipping, set-up new seed	10.0 cm long tube crystal, did not start c-axis single, bottom 5.5 cm a-axis, 100% β -alumina
H.P.-20AF†	Same	Same charge	Same charge	1.0	1 - 63	c-axis	Cracking appeared in tube 3 mm above die, emptied crucible	11.4 cm tube crystal, light blue color, poly α + β - alumina, 80% β
H.P.-21AF†	No shield on top of susceptor	20.0	9.1	1.0	1 - 2	c-axis	Four seeds broke before growth started, horizontal cracks, 3 mm above die	7.0 cm tube crystal 100% β -alumina, 7/8 c-axis at seeding 1/8 a-axis, badly cracked, deposit from growth
H.P.-22AF†	5-stack heat shield assembly on Mo susceptor	Same charge	Same charge	1.0	1 - 2	c-axis	Seed broke, setup new seed, tube cracked during growth	5.7 cm tube crystal, poly, 85% β - 15% α alumina, deposit from growth
H.P.23AF †	5-stack heat shield assembly on Mo susceptor	Same charge	Same charge	1.0	1 - 27	c-axis	Cracked during growth	10.8 cm tube crystal, poly, badly cracked, 35% β - 75% α-alumina
H.P.-24AF†	Ceramic setup, no after-heater	15.0	6 (H.P.)**	1.2	1 - 3	c-axis	Bad alignment, caused poor seeding - shield being picked up - aborted run	2.0 cm tube, contains α-patches on surface, poly c + a-axis β, white deposit on crystal

Table II. (continued)

Run No.	Afterheater Setup	Melt Composition (mole % Na_2O)	Charge Size (grams)	Gas Pressure (MN/m^2)	Growth Speed (mm/hr)	Seed Orientation	Comments	Results
H.P.-25AF†	Ceramic setup, two more shields	15.0	6 (H.P.)**	1.2 - 1.4	1	c-axis	New crucible, seed broke aborted run	6 mm tube crystal, α skin from being frozen to die
H.P.-26AF†	Ceramic setup, two more shields	15.0	Same charge	1.2 - 1.4	1 - 2	a-axis	Developed cracks, above top shield	3.5 cm tube crystal, poly, white deposit from growth, badly cracked 1% β - 99% α-alumina
H.P.-27AF	Ceramic setup, Al_2O_3 tube afterheater	15.0	Same charge	1.2	1 - 2	a-axis	Crystal kept freezing, crucible tilted, aborted run, crucible melted near bottom	3 mm piece - 100% α-alumina
H.P.-28AF	Mo susceptor, low in coil	15.0	6 (H.P.)**	1.2 - 1.4	1 - 9	a-axis	Seed broke, redipped, patchy area where tube connected, cracking	15.8 cm tube crystal, emptied crucible, poly $\alpha + \beta$, blackish deposit.
H.P.-29AF	Mo susceptor, high in coil	20.0	6.8	1.4	2 - 6	a-axis	Large meniscus, difficulty spreading to complete tube	13.2 cm tube crystal 100% β - alumina a-axis, gray deposit from growth run
H.P.-30AF	Mo susceptor, higher in coil	20.0	6.8	1.4	1 - 2	c-axis	Horizontal cracking ~2 mm above die, crystal froze, seed broke	1.1 cm long not complete tube, 100% β -alumina c-axis, slight cracks large facet where not connected tube
H.P.-31AF	Mo susceptor + 5-stack heat shields	20.0	Same charge	1.4	1 - 9	c-axis	Slight horizontal cracks ~2 mm above die, puller stalled, restarted	12.7 cm tube crystal, 100% β alumina c-axis first 10.0 cm; then a-axis, gray deposit from growth
H.P.-32AF	Mo susceptor + 7-stack heat shields	20.0	6.0	1.3 - 1.4	1 - 6	c-axis	Two seeds broke, slight cracks above top shield, crystal froze, seed broke, aborted run	10.0 cm long tube crystal, 100% β -alumina, started c-axis, α skin nucleated a-axis, deposit from growth
H.P.-33AF	Mo susceptor + 7-stack heat shields	Same charge	Same charge	1.3 - 1.4	1 - 4.5	c-axis	Patchy area on tube front before it becomes connected	Difficulty causing tube to close, froze, broke seed, 3 mm long, c-axis cleavage α-skin
H.P.-34AF	Mo susceptor + 5 stack heat shields	Same charge	Same charge	1.4	1 - 18	c-axis	Patchy area formed on tube ~ 2 mm above die	Emptied crucible, 10.0 cm tube crystal, 100% β, a + c-axis, α-patches, deposit on tube

Table II. (continued)

Run No.	Afterheater Setup	Melt Composition (mole % Na_2O)	Charge Size (grams)	Gas Pressure (MN/m^2)	Growth Speed (mm/hr)	Seed Orientation	Comments	Results
H.P.-35AF	Mo susceptor + 5 stack heat shields	20.0	6.8	1.3 - 1.4	1 - 2	c-axis	Broke two seed dipping slight horizontal cracking, large meniscus	15.0 cm tube crystal, 100% β -alumina, c-axis single, gray deposit on tube
H.P.-36AF	Mo susceptor + 5 stack heat shields	15.0 + 2 w/o MgO	6.8	1.3 - 1.4	1	c-axis	Seed broke at dipping, new seed, kept encountering freezing problem, aborted run	3 mm long, not complete tube, c-axis cleavage, α-skin
H.P.-37AF	Mo susceptor + 5 stack heat shields	Same charge	Same charge	1.3 - 1.4	1 - 24	c-axis	Seed broke, new seed patchy area on front of tube after 5 cm of growth	16.3 cm tube, 100% β - alumina, first 5 cm, c-axis then α-Al_2O_3 patch nucleated a-axis grain, deposit
H.P.-38AF	Mo susceptor + 5 stack heat shields	Same charge	Same charge	1.3 - 1.4	1 - 27	c-axis	X-tal froze, aborted run early	2 cm long tube, 100% β - alumina, poly a + c-axis
H.P.-39AF	Mo susceptor + 5 stack heat shields	Same charge	Same charge	1.3 - 1.4	1 - 27	c-axis	Froze to die, ended run	7 cm tube, coated with gray deposit from growth run, poly, $\alpha + \beta$-alumina
H.P.-40AF	Mo susceptor + 5 stack heat shields	15.0	5.0 (H.P.)**	1.3 - 1.4	1 - 6	c-axis	Seed broke, kept having freezing problems, aborted run	1 cm long, 3 mm complete tube, poly $\alpha + \beta$-alumina
H.P.-41AF	Mo susceptor + 5 stack heat shields	Same charge	Same charge	1.3 - 1.4	2 - 27	c-axis	Run emptied crucible of material	18.0 cm long tube, poly $\alpha + \beta$-alumina, gray deposit from growth

*450 kHz 20 KW induction unit
†10 Kc 20 KW motor generator
**High purity laboratory prepared starting material 99.999% Al_2O_3 microspheres and 99.999 sodium carbonate.

Table III. Ribbon Growth

Run No.	Afterheater Setup	Melt Composition (mole % Na_2O)	Charge Size (grams)	Gas Pressure (MN/m^2)	Growth Speed (mm/hr)	Seed Orientation	Comments	Results
H.P.-R1	Mo susceptor, 5-stack heat shields	20.0	6.8	1.3 - 1.4	1	c-axis	Ribbon kept freezing, broke seed	6 mm long ribbon crystal, c-axis single., α-skin patch, rest 100% β
H.P.-R2	Mo susceptor, 5-stack heat shields	Same charge	Same charge	1.4	1	c-axis	Freezing caused seed to break, ended run	3 mm long piece of c-axis, single, 100% β -alumina, very clear
H.P.-R3	Mo susceptor, 5-stack heat shields	Same charge	Same charge	1.4	1 - 3 - 1	c-axis	Faster speed caused large meniscus and ribbon to grow smaller than die	3.6 cm ribbon crystal, 100% β -alumina, c-axis single, very clear at bottom, gray deposit from growth
H.P.-R4	Mo susceptor, 5-stack heat shields	Same charge	Same charge	1.3 - 1.4	2 - 6 - 2	a-axis*	c-axis 90° to ribbon edge, ribbon has opaque patch on top front face	10.0 cm ribbon crystal, 100% β -alumina a-axis single, small crack up middle, α-patch at top, gray deposit.
H.P.-R5	Mo susceptor, 5-stack heat shields	Same charge	Same charge	1.4	1 - 27	c-axis	Seed broke upon dipping. Set new seed, ribbon does not appear clear as it grows	17.7 cm long ribbon, emptied crucible, poly α + β-alumina, gray deposit from growth.
H.P.-R6	Mo susceptor, 5-stack heat shields	30.0	6.8	1.35 - 1.4	1.0	c-axis	Ribbon did not look clear while growing, seed broke	3.8 cm long ribbon, opaque in color, not single, gray deposit from growth
H.P.-R7	Mo susceptor, 5-stack heat shields	Same charge	Same charge	1.55	1-2	c-axis	Ribbon does not look clear, will not grow size of die	6.0 cm long, opaque two phase, gray deposit from growth run
H.P.-R8	Mo susceptor, 5-stack heat shields	Adjusted charge to 20.0	6.8 Adjusted charge	1.35 - 1.4	1 - 9	c-axis	Ribbon appeared to be growing clear for 3.8 cm then less clear, froze	9.5 cm long ribbon, gray deposit from growth, c-axis β for 3.8 cm., then poly a and c-axis, crystal badly cracked
H.P.-R9	Mo susceptor, 5-stack heat shields	Same charge	Same charge	1.4	6 - 27	c-axis	Grew to empty crucible, ran out of pulling stroke	20.0 cm long ribbon, started c-axis single first 2.5 cm then poly α + β, gray coating from growth run
H.P.-R10	Mo susceptor, 5-stack heat shields	Same charge	Same charge	1.1 - 1.4	6 - 27	c-axis	X-tal froze, redipped, crucible emptied	8.4 cm long ribbon, α + β-alumina, cracked up middle, deposit from growth

Table III. (continued)

Run No.	Afterheater Setup	Melt Composition (mole % Na_2O)	Charge Size (grams)	Gas Pressure (MN/m^2)	Growth Speed (mm/hr)	Seed Orientation	Comments	Results
H.P.-R11	Mo susceptor, 5-stack heat shields	20.0	6.8	1.3 - 1.4	1	c-axis	Seeded, left to grow over night, seed caught on shield, broke	No crystal, 14 hrs at growth temperature
H.P.-R12	Mo susceptor, 5-stack heat shields	Same charge	Same charge	1.3 - 1.45	1 - 2	c-axis	Cleaned gray deposit from chamber, patchy area on top two sides of ribbon face	3.2 cm long ribbon, 100% β-alumina, poor seeding nucleated a-axis poly growth transparent patches at top gray deposit from growth.
H.P.-R13	Mo susceptor, 5-stack heat shields	Same charge	Same charge	1.5	1 - 3	c-axis	Patchy area on right side of ribbon face just after	3 mm long, exhibits c-axis cleavage, α-skin on right front side
H.P.-R14	Mo susceptor - one shield	Same charge	Same charge	1.55	2 - 275	c-axis	Grew very clear, small meniscus, some bubbles in crystal, increased speed after 1.2 cm of growth	Did not start single c-axis, two a-axis grains nucleated, poly 100% β-alumina at high growth speed, gray deposit on ribbon, 22.0 cm long, clear area cracked.
H.P.-R15	Mo susceptor - one shield	Same charge	Same charge	1.55 - 1.5	12 - 27	a-axis*	Grew very clear until speed increased, ribbon froze	5.7 cm long ribbon, not single, as three grains nucleated on seeding, 100% β-alumina, very clear 1.9 cm, then cloudy, covered with gray deposit, cracked where grains meet
H.P.-R16	Mo susceptor - one shield	Same charge	Same charge	1.6 - 1.5	12 - 38	a-axis*	Increased speed after 6 mm of growth, ribbon froze, seed broke, aborted run	5.5 cm long ribbon, 100% β-alumina, not single, several a-axis grains, very clear 6 mm, then milky, gray deposit on ribbon
H.P.-R17	Mo susceptor - one shield	20.0	6.8	1.45	1 - 18	a-axis*	Freezing problems, ribbon developed cracks ~2 mm above Mo shield, developed vertical cracks when growth terminated	5.0 cm ribbon crystal, fairly transparent, 100% β-alumina, several a-axis grains large vertical crack, gray deposit on ribbon
H.P.-R18	3-stack Mo heat shield assembly	Same charge	Same charge	1.55 - 1.45	1 - 18	a-axis*	Heated ribbon crystal to melt off of die and terminate run, caused internal flaws	5.0 cm ribbon, fairly transparent, 100% β-alumina, not single, several a-axis grains, cracked, gray coating

Table III. (continued)

Run No.	Afterheater Setup	Melt Composition (mole % Na_2O)	Charge Size (grams)	Gas Pressure (MN/m^2)	Growth Speed (mm/hr)	Seed Orientation	Comments	Results
H.P.-R19	3-stack Mo heat shield assembly	Same charge	Same charge	1.55 - 1.45	1 - 18	a-axis*	Poor seeding, started again, would not grow size of die at faster speed, aborted run	3.2 cm ribbon, 100% β - alumina, a-axis single, clear, not uniform width, slight vertical cracks, gray deposit on ribbon
H.P.-R20	Set up higher in coil - 6 mm	Same charge 15.0 +2 w/o MgO	Same charge	1.55 - 1.45	1	a-axis* tube seed	Seed broke on dipping, new seed c-axis tube on side, could not grow, freezing problems, crucible overheated - melted	2 mm long piece, very clear, single a-axis, 100% β - alumina
H.P.-21	3-stack Mo shields, higher in coil	0.15 +2 w/o MgO	6.8	1.4	1 - 4.5 - 27	a-axis* tube seed	Tube seed prevented clear view at seeding, grew first 10.0 cm at 4.5 mm/hr, ran out of pulling stroke	19.5 cm long ribbon, 100% β -alumina, not single, cold start nucleated several a-axis grains, clear, two large cracks, gray surface deposit
H.P.-R22	3-stack Mo shields, 6 mm lower in coil	Same charge	Same charge	1.4	1 - 27	a-axis* tube seed	Dipped hot, after 6 mm of growth cloudy area formed on ribbon edge	10.0 cm long ribbon, started a-axis single for 1.9 cm, α-Al_2O_3 patch, slight crack, rest $\alpha + \beta$ alumina, gray deposit
H.P.-R23	3-stack Mo shields, 3 mm higher in coil	Same charge	Same charge	1.55 - 1.45	1 - 27	a-axis*	Cloudy area on ribbon face +edges, difficulty growing size of die, emptied crucible	5.0 cm long ribbon, poly $\alpha + \beta$ -alumina, α-skin patches +opaque inclusions, not size of die, gray deposit
H.P.-R24	3-stack Mo shields, lower in coil	16.3 +5 w/o MgO	6.8	1.55 - 1.45	1 - 3 - 27	a-axis*	Ribbon cracked as it grew above top shield, turned poly at 27 mm/hr, 6 mm long	3.8 cm long ribbon, cracked up middle top to bottom, not single, several a-axis grains, very clear, gray surface deposit
H.P.-R25	3-stack Mo shields, lower in coil	Same charge	Same charge	1.55 - 1.45	1 - 27	c-axis	Grew in c-axis to see if this would prevent vertical cracking, after 1.2 cm of growth ribbon did not appear to be c-axis	13.3 cm ribbon, ribbon cracked when removed from die, c-axis first 6 mm then shifted a-axis , after 1.9 cm single a-axis, quite clear, gray deposit

Table III. (continued)

Run No.	Afterheater Setup	Melt Composition (mole % Na_2O)	Charge Size (grams)	Gas Pressure (MN/m^2)	Growth Speed (mm/hr)	Seed Orientation	Comments	Results
H.P.-R26	Mo susceptor, 5-stack heat shield	Same charge	Same charge	1.55 - 1.45	1 - 12	a-axis*	3 mm between, first and second shield to try and prevent vertical cracking	5.5 cm ribbon, started single but after 5 mm sec phase nucleated three grains, cracked where grains met, very clear, gray coating on ribbon
H.P.-R27	Slotted 6-stack heat shield assembly	Same charge	Same charge	1.45	1 - 27	a-axis*	Slotted heat shields to try and even temperature gradient, looks cloudy where seeded	Emptied crucible, 12.7 cm ribbon, second phase nucleated several a-axis grains cracked at top middle, uncracked at bottom, clear, gray deposit
H.P.-R28	Slotted 6-stack heat shield assembly	16.8 +2 w/o MgO	6.8	1.55 - 1.45	1 - 6	a-axis*	Top of ribbon cloudy, difficult to grow size of die, did not crack	3.8 cm ribbon, first 4 mm contains second phase, started single, then it developed two a-axis grains, 1.5 cm size of die, rest not, uncracked, gray deposit from growth.
H.P.-R29	Slotted 6-stack heat shield assembly	Same charge	Same charge	1.55 - 1.45	3	a-axis*	Ribbon does not appear single after 1.2 cm	10.0 cm ribbon, cracked where two a-axis grains meet, last 3.8 cm very clear, above gray coating, 100% β
H.P.-R30	Slotted 6-stack heat shield assembly	Same charge	Same charge	1.55 - 1.45	6	a-axis*	White area on right hand edge of ribbon just after seeding, does not appear single, seed broke	5.1 cm ribbon, quite clear, contains internal second phase, not cracked, not single, gray coating, before anneal.
H.P.-R31	Slotted 6-stack heat shield assembly	Same charge	Same charge		3 - 12	a-axis*	Does not appear single, growth emptied crucible	16.0 cm ribbon, not single, contains second phase, $\alpha+\beta$ -alumina, not cracked, gray coating from growth
H.P.-R32	Slotted 6-stack heat shield assembly - 6 mm higher in coil	16.9 +2 w/o MgO**	5.8**	1.55 - 1.45	3 - 12	a-axis*	Seed broke dipping, new seed, spread slowly	10.0 cm long ribbon, a-axis single, 100% β -alumina, uncracked, fairly clear, gray deposit from growth

Table III. (continued)

Run No.	Afterheater Setup	Melt Composition (mole % Na_2O)	Charge Size (grams)	Gas Pressure (MN/m^2)	Growth Speed (mm/hr)	Seed Orientation	Comments	Results
H.P.-R33	Slotted 6-stack heat shield assembly - 6 mm higher in coil	Same charge	Same charge	1.55 - 1.45	3 - 15	a-axis*	Ribbon froze after 3.5 cm, heated and increased pulling speed to 15 mm/hr, grew overnight	15.2 cm ribbon crystals, not size of die for more than 6.3 cm, then tapered to point, a-axis single, 100% β -alumina, gray deposit on surface, before anneal, uncracked.
H.P.-R34	Slotted 6-stack heat shield assembly - 6 mm higher in coil	Same charge	Same charge	1.55 - 1.45	3 - 20	a-axis*	Ribbon froze during night, causing seed to break	4.5 cm ribbon, uncracked, not single, $\alpha + \beta$ -alumina, α-skin coatings
H.P.-R35	Slotted 6-stack heat shield assembly - 6 mm higher in coil	Same charge	Same charge	1.55 - 1.45	6 - 27	a-axis*	Growth emptied crucible	11.4 cm ribbon, whitish opaque, poly $\alpha + \beta$ -alumina, annealed to remove gray coating
H.P.-R36	Iridium susceptor, 5-stack slotted shields	16.9 +2 w/o MgO**	6.8**	1.55 - 1.45	3 - 6	a-axis*	5-stack shield assembly became tilted, shut down to realign, part of seed broke, redipped, ribbon picking up shield, aborted run	0.47 cm ribbon, single, very clear, a-axis, 100% β -alumina, not size of die
H.P.-R37	Iridium susceptor, 5-stack slotted shields	Same charge	Same charge	1.55 - 1.45	3 - 12 - 6	a-axis*	After ~2.5 cm, ribbon started to cut in at 12 mm/hr slowed to 6 mm/hr	6.3 cm ribbon, size of die for 2.5 cm, then smaller for 0.9 cm, then size of die, a-axis single, clear, slight crack, white coating from growth, before anneal
H.P.-R38	One less iridium shield	Same charge	Same charge	1.55 - 1.45	3 - 6	a-axis*	Ribbon froze, seed broke, aborted run	2.5 cm ribbon, a-axis single, clear, uncracked, 100% β -alumina, white coating before anneal
H.P.-R39	One less iridium shield - 6 mm higher in coil	Same charge	Same charge	1.55 - 1.45	3 - 6 -18	a-axis*	Ribbon started to freeze, nucleated 2nd grain, slight vertical crack in middle	6.2 cm long ribbon, two a-axis grains, 100% β -alumina, slight vertical crack in middle, clear, white coating from growth run.

*c-axis 90° to ribbon edge
**Monofrax H was selected high quality clear crystal.

IV. CRYSTAL GROWTH EXPERIMENTS

A. Discussion and Objectives

Crystal structure analysis of β-alumina indicates an "ideal" stoichiometry $Na_2O \cdot 11\ Al_2O_3$ (8.33 mole % Na_2O). However, analyses by many investigators have shown that the compound usually contains more than the "ideal" quantity of Na_2O. In the $NaAlO_2$- Al_2O_3 diagram of Weber and Venero (Fig. 3), for example, the β-alumina phase field is shown with a breadth corresponding to 10.0 to 11.2 mole % Na_2O. More recently, Harata[16] reported that the single phase region extends from 10.9 to 13.7 mole % Na_2O.

There are considerable difficulties associated with the crystal growth of sodium beta-alumina including its peritectic formation from slightly soda-rich liquid and α-alumina at about 2240 ± 6°K[15, 19] and the ~ 5 torr pressure of Na_2O vapor over β-alumina[2] at the peritectic temperature. To limit the loss of Na_2O from the melt and hot crystal, growth was conducted in a high pressure chamber containing 1.1 to 1.6 MN/m^2 argon (Figs. 1, 2). Excess Na_2O was placed in the crucible charge (see Table III). This compensated for vapor losses and depressed the freezing temperature below the peritectic temperature.

To grow crystals of different compositions, both melt composition and chamber pressure were varied (Table II). Because the solidus in the soda-rich region has a finite slope (Fig. 3), it was also possible to obtain crystals with differing Na_2O content by varying the freezing temperature via melt composition in the range of 10 to 35 mole % Na_2O. The Na_2O concentration in the liquid of the meniscus was determined by the balance of the rates of rejection from the interface and depletion by vaporization. The composition of crystals grown by this technique is therefore extremely rate dependent (see Fig. 6).

Fig. 6. Compares Debye-Scherrer films of (from top to bottom) 100% beta-alumina, beta-alumina and sodium beta alumina β " and sodium magnesium beta-alumina and sodium magnesium β ". Top film: Debye-Scherrer of H.P.-10AF; middle film: H.P.-10AF bottom and bottom film: Debye-Scherrer of H.P.-R24 top

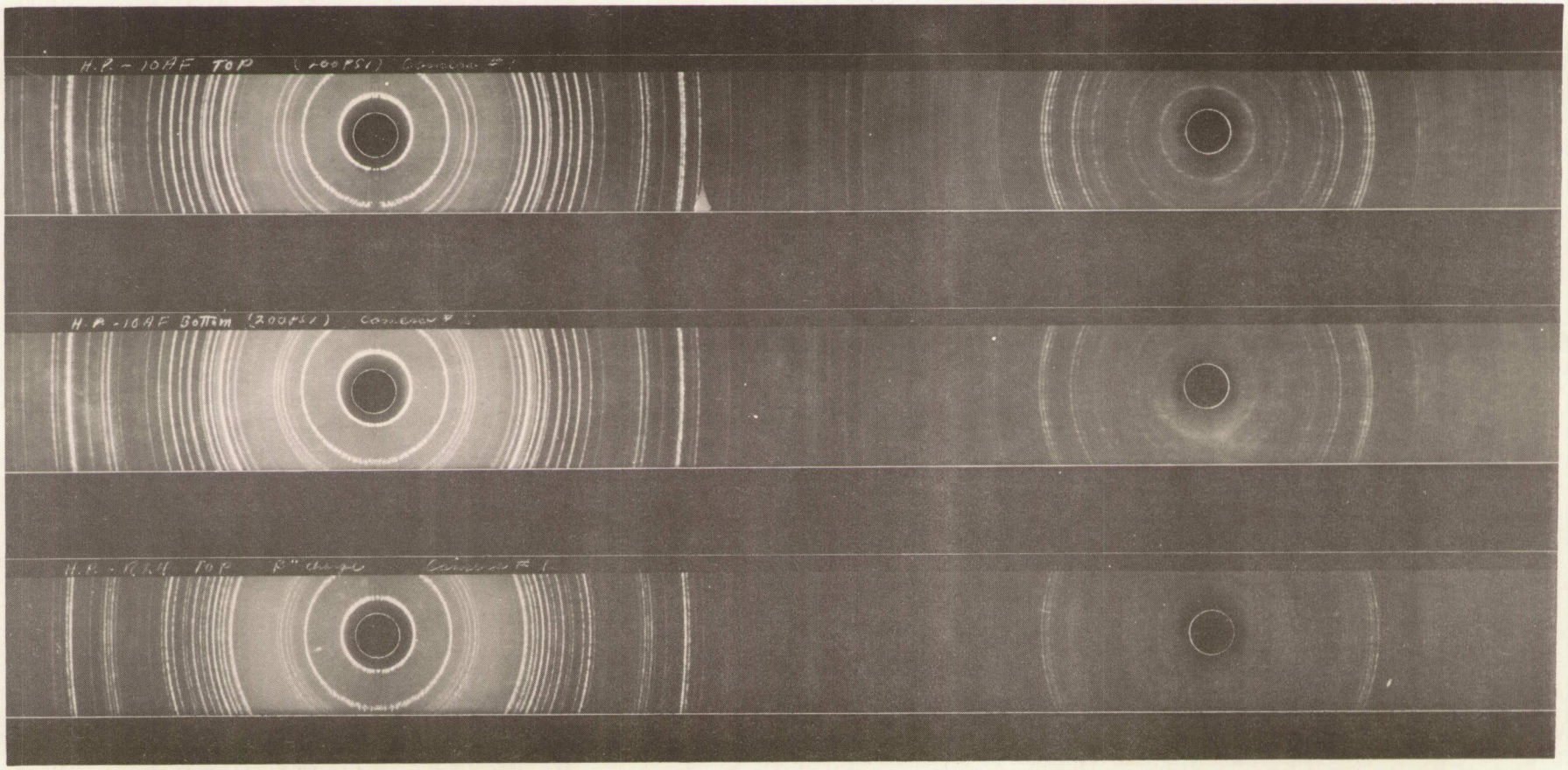

Some of the crystals grown under the preceding contracts[6, 7] cracked in the steep temperature gradient above the die. Under this program an attempt to alleviate the cracking problem was made by the use of an afterheater. The afterheater in several cases was a metal tube heated by induction from the same rf source that heated the crucible and in some cases was a series of stacked disk shields. Numerous growth trials were necessary to achieve an optimum design (see Table II, III).

Another problem encountered in the preceding work was the condensation of Na_2O vapor on the cooler regions of the crystal. The afterheater was effective in reducing this problem by increasing the distance between the source of the Na_2O vapor and the cool crystal surfaces. Baffles or shields were also used to try and trap the condensing vapor.

Both a-axis and c-axis tubes of β-alumina have been grown. Two phase mixtures of α and β-alumina resulted when the melt was soda-poor. Because the presence of a high tensile strength second phase such as α-alumina was hoped might strengthen a β-alumina crystal without seriously degrading its conductivity, some mixed α-β crystals were prepared for study.

B. Results

1. Sodium β-alumina tubes

Table II lists all the afterheater arrangements and growth variables used for the growth of beta-alumina tubes. It can be seen from Table II, that although the use of a suscepting tube afterheater prevented cracking and the soda-rich deposit from forming on the tubes, it had the detrimental effect of causing opaque white skin patches to form on the tubes. Figs. 7a, and 7b, show a tube with the opaque white skin patch formed at the top. At faster growth speeds the opaque no longer formed, but the tube crystal started to pick up a second phase. The isolated opaque skin patch was found by the Debye-Scherrer X-ray technique to be α-Al_2O_3. The rest of the tube was beta-alumina.

Several growth experiments were performed from an 18 mole % soda-rich melt using no afterheater (Table II). The tubes were grown in both the a- and c-axis and all but one resulted in 100% beta-alumina. All the tubes were covered with a grayish-white deposit which was removed by heat treating at 1523°K (e.g., above the decomposition temperature of Na_2O). Fig. 8 shows the results of these growth runs. As can be seen from the photograph the tube crystals became less transparent with

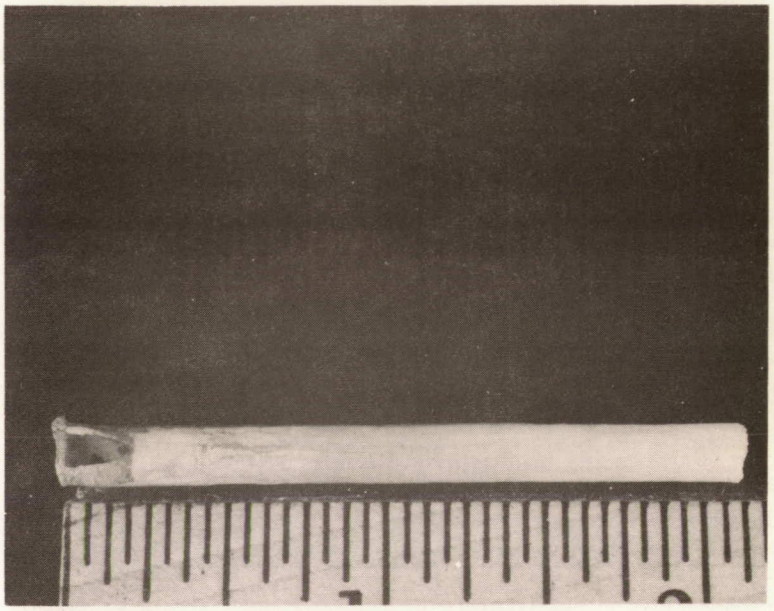

Fig. 7a. Sodium beta-alumina tube H.P.-1AF front, showing white poly α-Al_2O_3 skin

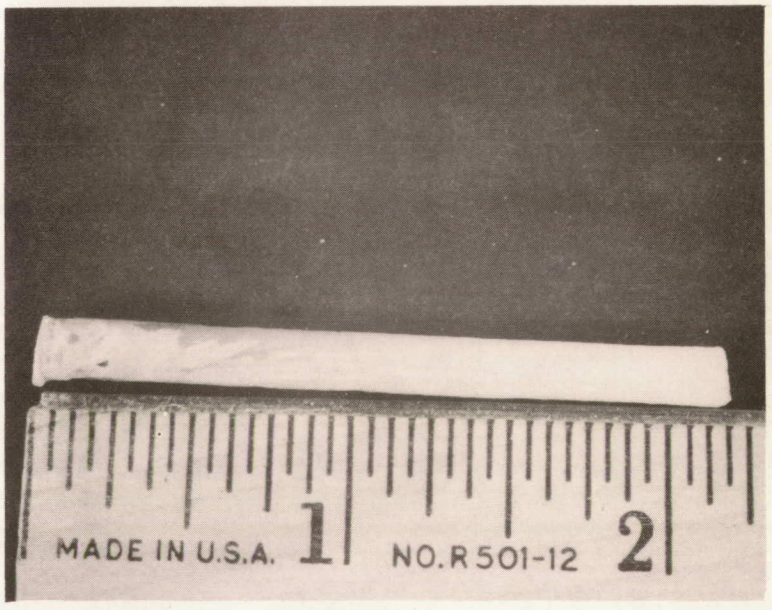

Fig. 7b. Sodium beta-alumina tube H.P.-1AF back, showing white poly α-Al_2O_3 skin

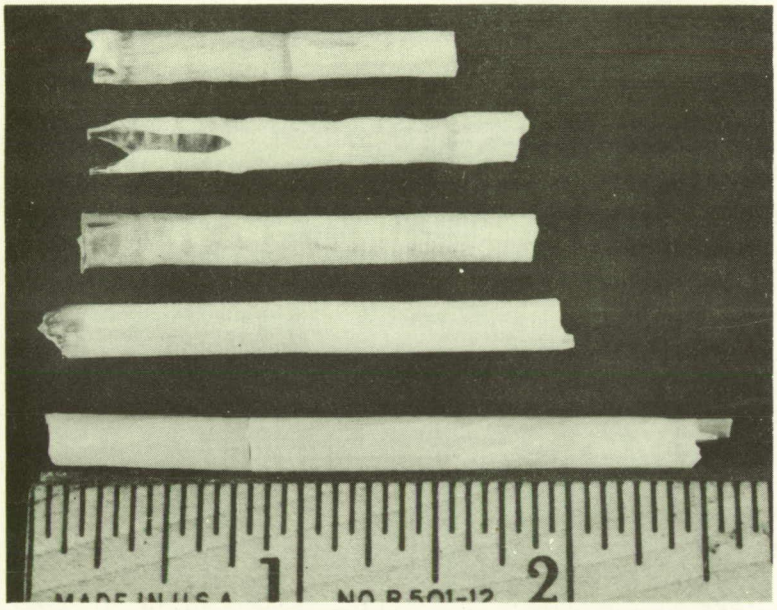

Fig. 8. From top to bottom: sodium beta-alumina tube crystal H.P.-7AF, H.P.-8AF, H.P.-9AF, H.P.-10AF and H.P.-11AF

increasing length and growth speed. Debye-Scherrer X-ray samples, taken from the top of the first four tubes in this photograph showed 100% beta-alumina, samples taken from the bottom showed beta alumina plus weak lines of a second phase. These lines were found to belong to the soda-rich β'' phase (Figs. 6 and 9). Although the phase diagram by Weber and Venero[15] (Fig. 3) shows soda-rich β'' to be a metastable compound which does not exist above 1873°K, we have found it to co-exist with β-alumina grown above 2200°K in several of our growth experiments. This is apparently due to the fact that the growth process does not take place at equilibrium.

Although several advantages using 10 kHz instead of rf induction heating were realized, some difficulties were encountered in reestablishing the original optimized gradients (due in part to the new coil configuration and in part to the deeper skin effect induced by the lower frequency field).

In order to establish the optimum conditions for the growth of single crystal beta-alumina tubes several growth experiments were performed using 1.5 to 2 g charges. It was found that the soda loss was too high from these small charges to obtain 100% beta-alumina (Table II). A 100% β-alumina tube (H.P.-19 AF) was grown from a 6-g charge of 13 mole % Na_2O at ~1.0 MN/m^2. It was seeded in the c-axis direction but was found after ~1.2 cm to have spontaneously changed orientation and grown in the a-axis direction (Fig. 10). The second tube crystal grown from this charge resulted in a mixture of ~80% β - 20% α-alumina (Fig. 10). Table IV shows that tube crystal H.P.-20 AF contains less soda then required for 100% beta-alumina and tube crystal H.P.-19AF contains slightly more.

A growth experiment was performed from a 9.0-g melt of $(Na_2O)_{0.2}$ $(Al_2O_3)_{0.8}$ duplicating as closely as possible the conditions that had previously produced single crystal 100% beta-alumina tubes.[6, 13] The only deviation was that the pressure during growth was 1.0 MN/m^2 instead of 1.4 MN/m^2. The tube crystal that resulted (H.P.-21AF) was 100% beta-alumina and mostly c-axis but was badly cracked. A second growth run (H.P.-22AF) from the same melt and using a Mo heat shield arrangement to prevent cracking, along with the previous growth parameters, resulted in a tube of ~85% β, 15% α-alumina (Table IV). A growth pressure of at least 1.4 MN/m^2 appears necessary to obtain more than one 100% beta-alumina tube crystal 4.0 cm long, from at least a 6.0 g charge.

Fig. 11 shows two 100% beta-alumina tube crystals grown from a 6.8 g charge with the composition $(Na_2O)_{0.2}$ $(Al_2O_3)_{0.8}$ The tube crystal H.P.-29AF was grown

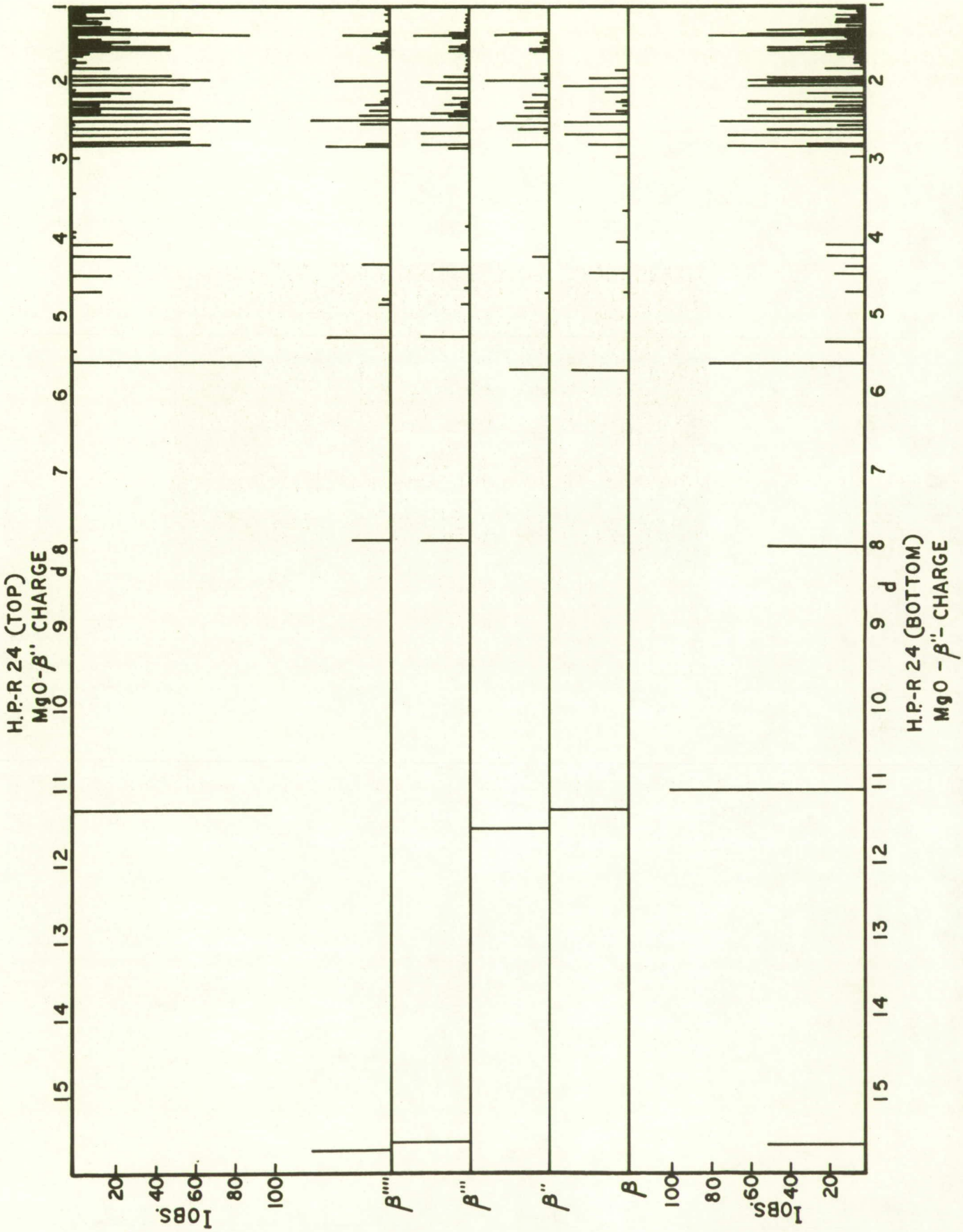

Fig. 9. X-ray spectrum of β , β '', β ''' and β '''' compared to x-ray spectrum from Debye-Scherrer films of H.P.-R24 (top) and H.P.R24 (bottom) grown from a melt of sodium magnesium β ''

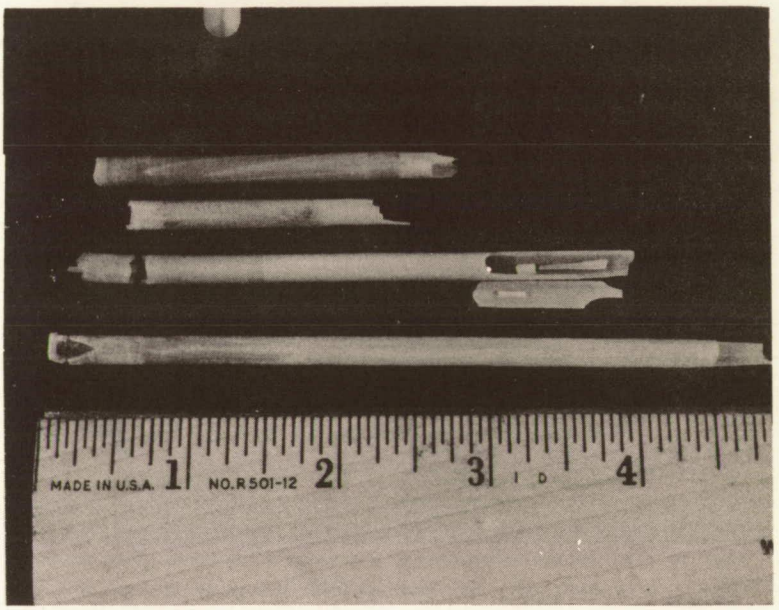

Fig. 10. From top to bottom: sodium beta-alumina tube crystal H.P.-13AF, H.P.-14AF, H.P.-19AF and H.P.-20AF

Table IV. Composition of Tube Crystals

Crystal		Analysis (wt %)			Mole %	
		Na	Al	O	Na_2O	Al_2O_3
H.P.-19AF	Charge				13.0	87.0
	Top	4.1	51.4	(44.4)	8.56	91.4
	Bottom	4.49	51.2	(44.31)	9.33	90.6
H.P.-20AF	Charge				13.0	87.0
	Top	3.72	53.1	43.18	7.6	92.4
	Bottom	3.37	53.3	43.33	6.9	93.1
H.P.-22AF	Charge				20.0	80.0
	Top	3.23	51.7	(45.07)	6.8	93.2
	Bottom	3.63	53.0	(43.37)	7.4	92.6
H.P.29AF	Charge				20.0	80.0
	Top	4.30	51.6	(44.1)	8.9	91.1
	Bottom	4.40	52.0	(43.6)	9.0	91.0
H.P.-31AF	Charge				20.0	80.0
	Top	4.33	50.4	(45.27)	9.2	90.8
	Bottom	4.33	50.8	(44.82)	9.1	90.9
H.P.-35AF	Charge				20.0	80.0
	Top	5.10	51.8	(43.1)	10.4	89.6
	Bottom	5.40	50.4	(44.2)	11.2	88.8

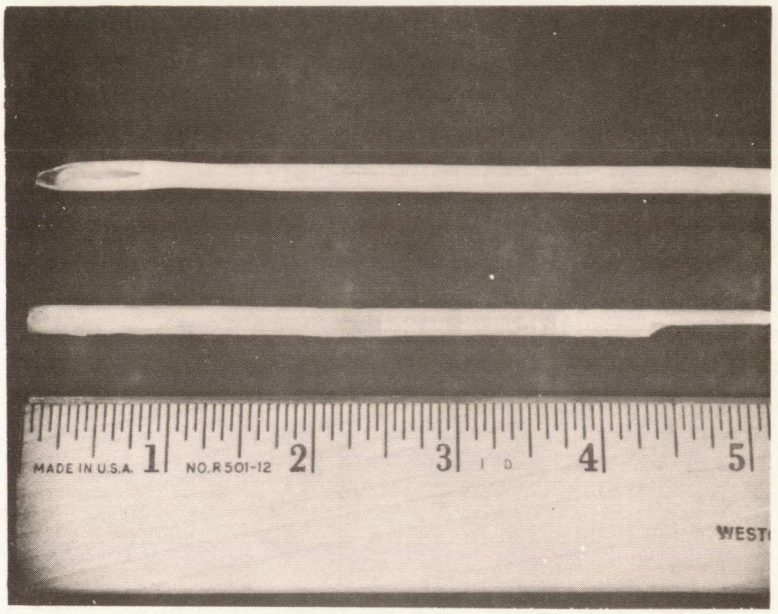

Fig. 11. Top: 100% sodium beta-alumina a-axis tube H.P.-29AF, bottom: 100% sodium beta-alumina c-axis tube H.P.-31AF

in the a-axis direction at 6.3 mm/hr after it became a full tube. No afterheater was used and it exhibited slight vertical cracking. Fig. 12 is a Laué back-reflection photograph taken of a facet on the top area of tube H.P.-29AF, 90° to the tube axis which exhibits the c-plane. The second crystal H.P.-31AF was grown in the c-axis direction at a speed of 2 mm/hr for 6 cm, then 6 mm/hr for the next 2.5 cm and finally 9 mm/hr for the remainder of the crystal. The use of a heat shield assembly did not prevent slight horizontal cracking of the tube crystal which was, however, single and orientated in the c-axis direction. Tube crystal (H.P.-35AF) with a higher sodium content then H.P.-29AF or H.P.-31AF was also grown from a melt of $(Na_2O)_{0.2}(Al_2O_3)_{0.8}$ but at a growth speed of only 1 to 5 mm/hr (Table II and IV).

Although the use of an excess Na_2O melt composition and a heat shielding arrangement, together with a high inert gas overpressure allowed the growth of single crystal sodium beta-alumina tubes at speeds up to 12 mm/hr, the majority of the crystals did develop slight cracks and all had grayish white surface deposits which had to be removed by heat treating.

2. Sodium magnesium beta-alumina tubes

A considerable proportion of MgO can be incorporated into the β-alumina structure (up to the composition 6.5 MgO · 10.5 Na_2O · 83 Al_2O_3).[20] Higher MgO content (~ 10.0 mole %) changes the lattice to the β''-alumina structure (Fig. 4). Because of this phase latitude and the sensitivity of the conductivity to the Na^+ environment, particularly as affected by Mg ions, this effort included the growth of tubes with various amounts of MgO.

The techniques and equipment used to grow beta-alumina plus magnesium oxide tubes were the same as those mentioned above the growth of sodium beta-alumina (Table II). Growth was performed in the c-axis direction using a piece of Monofrax H single crystal as a seed, and growth was performed under 1.4 MN/m^2 argon overpressure at pulling speeds from 2 to 20 mm/h. The starting charge was 1.8 g made up of Monofrax H beta-alumina, Na_2O (in the form of Na_2CO_3) and MgO. The starting composition was $(Na_2O)_{15.67}(MgO)_{4.61}(Al_2O_3)_{79.92}$. Fig. 13 shows an MgO doped beta-alumina tube (H.P.-37AF). The tube is essentially a single crystal with the c-axis parallel to the growth direction. It is apparently no more difficult to grow beta-alumina with magnesium oxide than it is to grow undoped beta-alumina.

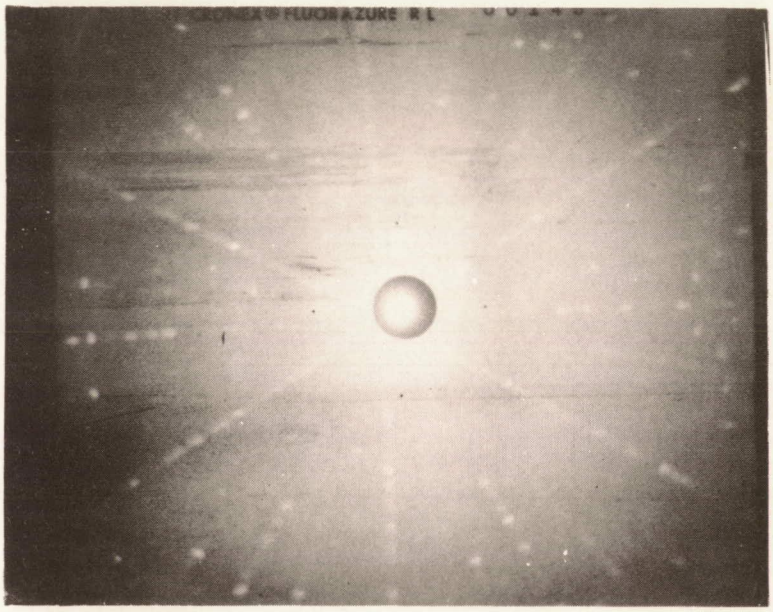

Fig. 12. Laué back reflection photograph taken (90° to tube axis) of top clear section (facet) of H.P. 29AF a-axis sodium beta-alumina tube

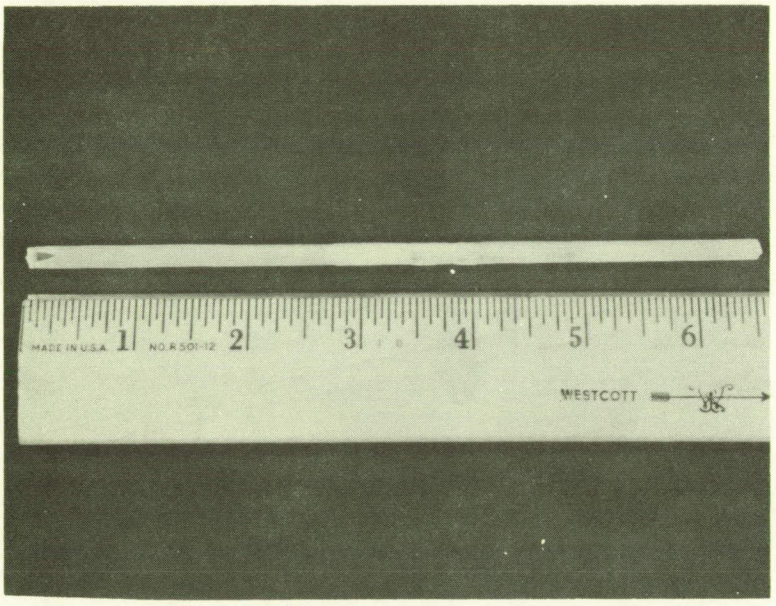

Fig. 13. Sodium magnesium beta-alumina c-axis tube

3. Sodium-beta-alumina ribbons

The growth of sodium beta-alumina ribbons was performed using the same growth techniques as those employed for the growth of sodium beta-alumina tubes (Table III). An iridium crucible and an iridium die designed to yield ribbons 6 mm wide $\times$ 0.8 mm thick were used. Fig. 14 shows two sodium beta-alumina ribbon single crystals grown at growth speeds of 1 to 6 mm/hr from the same 6.8 g charge of $(Na_2O)_{0.2}(Al_2O_3)_{0.8}$. As can be seen from the photograph, difficulty was encountered with keeping the ribbon crystals a uniform width at the faster growth speeds. This is attributed to the particular heat shield arrangement used. The c-axis crystal (H.P.-R3) developed cleavage cracks normal to the c-axis and the a-axis ribbon a- c-plane crack down the middle. There was an α-Al_2O_3 skin patch on the top of the a-axis ribbon. The ribbon crystals were less transparent after the heat treatment used to remove the grayish surface deposit. This can be seen by comparing the bottom clear section of H.P.-R3 (Fig. 14) with the rest of the ribbon. As this portion was still in the heat shields when growth was terminated it did not have a surface deposit and therefore was not heat treated. Fig. 15 is a photograph of three ribbon crystals grown at faster growth speeds (1 to 18 mm/hr) using two different shielding arrangements (Table III). Cracking was still a problem and the crystals also had horizontal bands of soda rich material. Table V lists the chemical composition of three 100% sodium beta-alumina ribbon crystals grown at different growth speeds. These ribbons are the third, fourth, and fifth growth runs from the same 6.8 g charge. As can be seen from Table V, ribbon crystal H.P.-R15 contains more Na_2O than the single phase limit for beta-alumina stated by Harata.[16] This is due to second phase inclusions trapped in the ribbon crystal during growth and was apparent by the ribbon crystals' cloudy appearance. Crystal H.P.-R14 also had second phase inclusions and was completely opaque.

These experiments seem to indicate that properly orientated single crystal sodium beta-alumina ribbons can regularly be produced at $\sim$2 mm/hr but cracking is still a problem and faster growth rates tend to cause several crystal grains to nucleate.

4. Sodium magnesium beta-alumina ribbons

Table III lists the parameters used for the growth of the sodium magnesium beta-alumina ribbon crystals. The iridium crucible and die had the same dimensions as those used for the growth of the previous ribbon crystals. A melt of

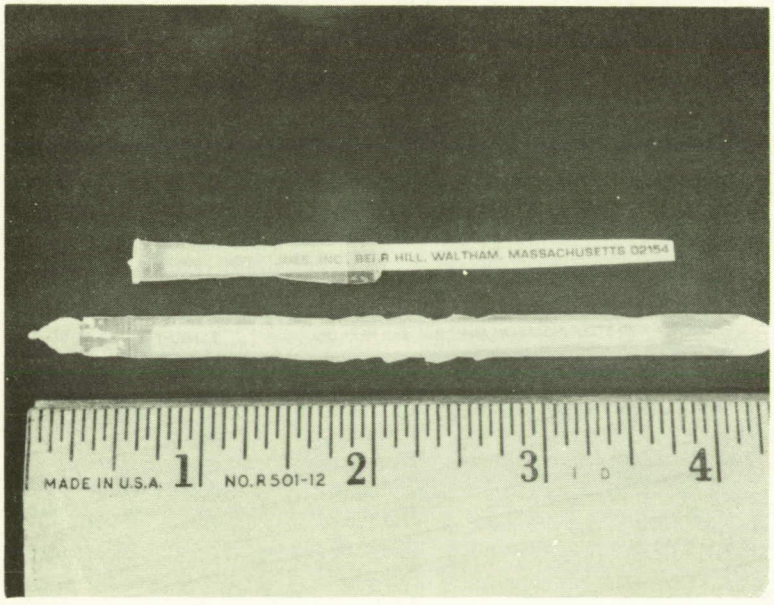

Fig. 14. Top: sodium beta-alumina single crystal c-axis ribbon; bottom: sodium beta-alumina single crystal a-axis ribbon, notice the poly α-skin patch at the top of the ribbon above the 4 in. mark

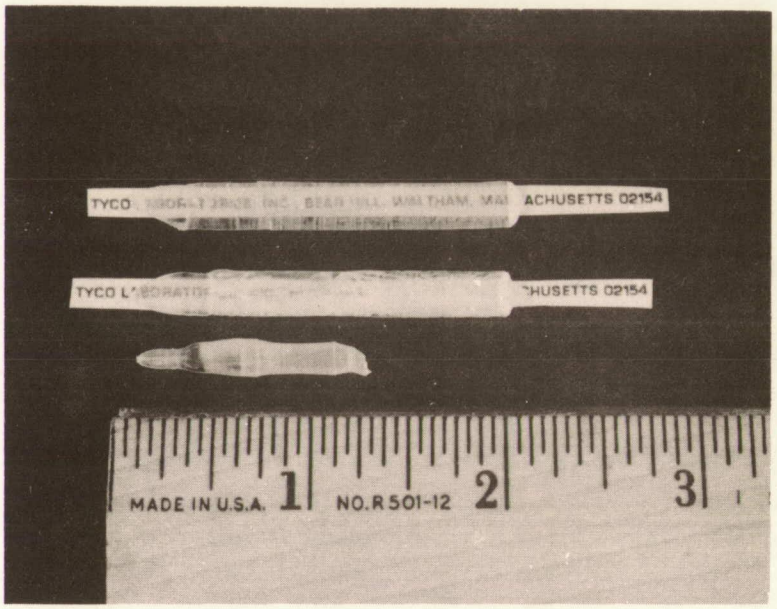

Fig. 15. From top to bottom: sodium beta-alumina ribbon a-axis ribbon crystal H.P.-R17, H.P.-R18 and H.P.-R19

Table V. Composition of Ribbon Crystals

Crystal		Analysis (wt %)				Mole %		
		Na	Mg	Al	O	Na_2O	M_gO	Al_2O_3
H.P.-R14	Charge					20.0		80.0
	Top	6.8		47.3	(45.9)	14.4		85.6
	Bottom	7.3		45.6	(47.1)	15.8		84.2
H.P.-R15	Charge					20.0		80.0
	Top	8.3		47.9	(43.8)	16.9		83.1
	Bottom	8.4		50.0	(41.6)	16.5		83.5
H.P.-R16	Charge					20.0		80.0
	Top	5.7		44.8	(49.5)	13.0		87.0
	Bottom	4.3		48.8	(46.9)	9.4		90.6
H.P.-R25	Charge					16.3	11.0	72.7
	Top							
	Bottom	5.6	1.14	-	-	-	-	-
H.P.-R32	Charge					16.9	4.6	78.5
	Top	6.9	0.69		-	-	-	-
	Bottom	5.7	0.44		-	-	-	-
H.P.-R33	Charge					16.9	4.6	78.5
	Top	6.9	0.77		-	-	-	-
	Bottom	5.4	0.30		-	-	-	-

the composition $(Na_2O)_{0.1426}(MgO)_{0.0452}(Al_2O_3)_{0.8121}$ and weighing 6.8 g was used for the growth of the first four ribbon crystals. This resulted in a badly cracked 100% beta-alumina ribbon. The next 6.8 g charge was richer in Na_2O and had the composition $(Na_2O)_{0.1694}(MgO)_{0.0458}(Al_2O_3)_{0.7848}$. Two 100% sodium magnesium beta-alumina ribbons were grown from this melt, they were not single and the second ribbon H.P.-R29 was badly cracked (Fig. 16). A third 6.8 g charge of the same composition as the previous was prepared using select single crystals of Monofrax H. From this two uncracked 100% sodium magnesium beta-alumina crystals were grown. The chemical compositions of two Na-Mg-β-alumina crystals (H.P.-R32 and H.P.-R33) are listed in Table V and Fig. 17. All of the ribbon crystals still had a grayish white surface deposit from growth which had to be removed by heating to ~ 1523°K.

On several occasions the coating was not completely removed by the heat treatment and a white powdery film remained. A part of this deposit problem appeared to have been caused by the Mo susceptor. A susceptor was fabricated out of iridium with the same dimensions as the Mo susceptor and a series of growth runs was made. Table III lists the parameters used and the results. Fig. 18 is a photograph of the results of these experiments. The average growth speed for the ribbons was > 6 mm/hr, the ribbons became less transparent with increased growth speed. There was very little cracking from the growth runs but the ribbons were coated with a white deposit where they grew above the heat shields. This deposit appeared to be slightly easier to remove by heating to 1523°K than the grayish white deposit. Compare Fig. 19 with Fig. 18.

5. Sodium magnesium β''-alumina Ribbons

Equilibrium phase information on Mg stabilized β'' alumina is limited. The phase is stable at least to 1800°C and has very little compositional freedom at 1700°C (Fig. 4).[20] Weber and Venero[20] grew crystals of Mg-β'' from NaO_2 rich melts by an isothermal treatment at 1650°C allowing the slow evaporation of Na_2O. Experience with the EFG growth of sodium magnesium beta-alumina tubes indicated that it was also necessary to grow magnesium β'' from Na_2O rich melts. The sodium magnesium β'' ribbon crystal growth runs were made from 6.8 g charges of $(Na_2O)_{0.1626}(MgO)_{0.1099}(Al_2O_3)_{0.7274}$ (Table III). Cracking due to thermal strain was observed in all of these crystals (see Fig. 19). This may have been due to the presence of more than one sodium aluminate phase. Fig. 9 shows Debye-

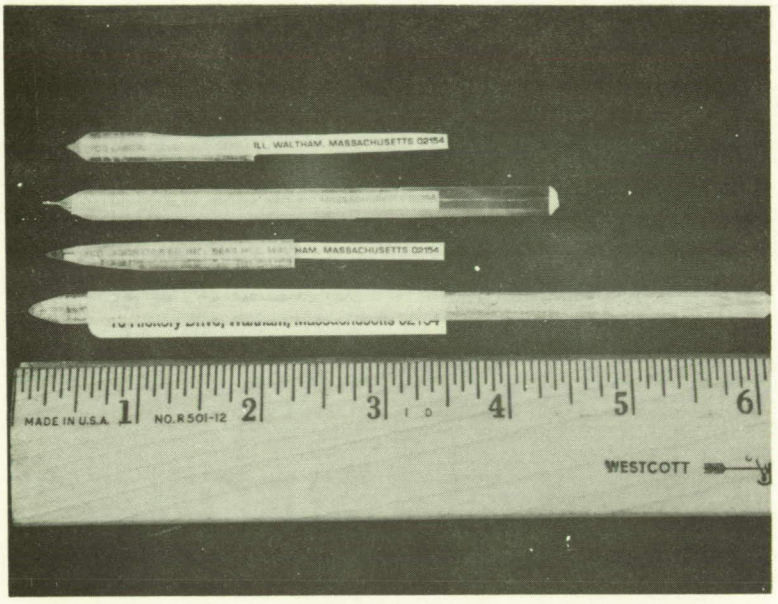

Fig. 16. From top to bottom: sodium magnesium beta-alumina a-axis ribbon crystal H.P.-R28, H.P.-R29, H.P.-R30 and H.P.-R31

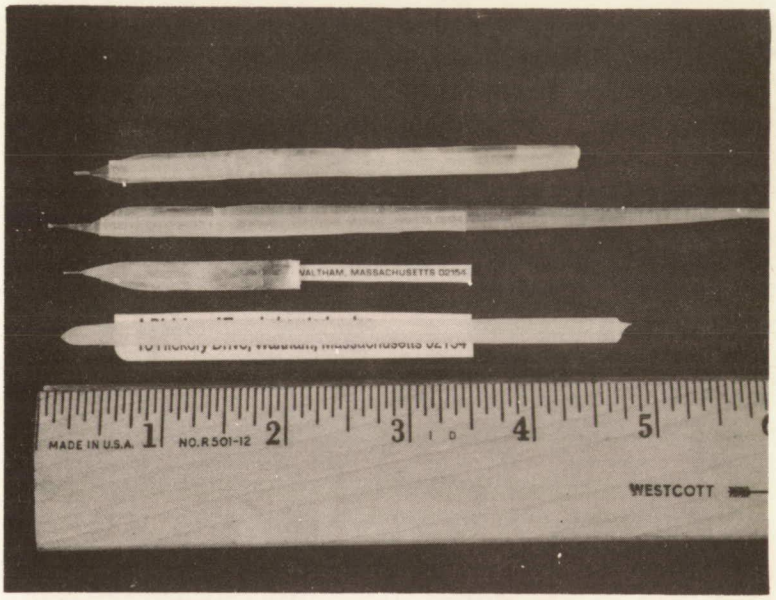

Fig. 17. From top to bottom: sodium magnesium beta-alumina a-axis ribbon H.P.-R32, H.P.-R33, H.P.-R34 and H.P.-R35.

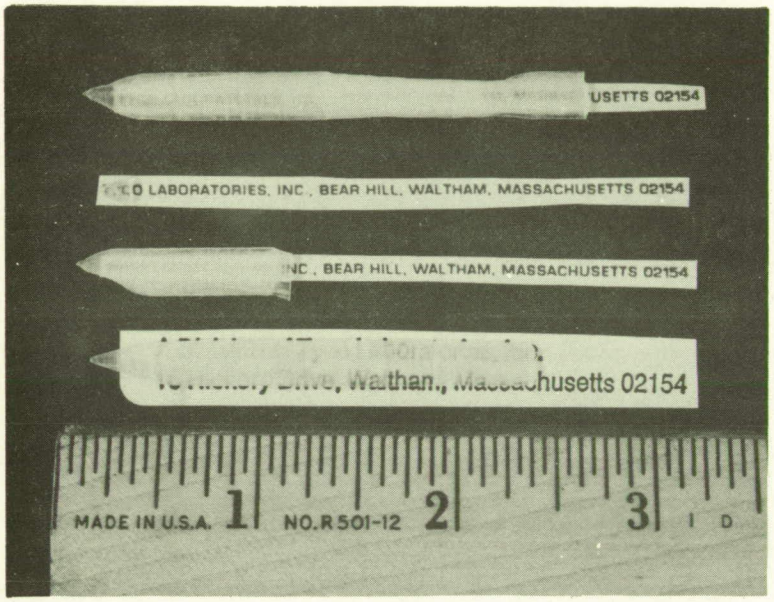

Fig. 18. From top to bottom: sodium magnesium beta-alumina ribbon H.P.-R37, H.P.-R36, H.P.-R38 and H.P.-R39

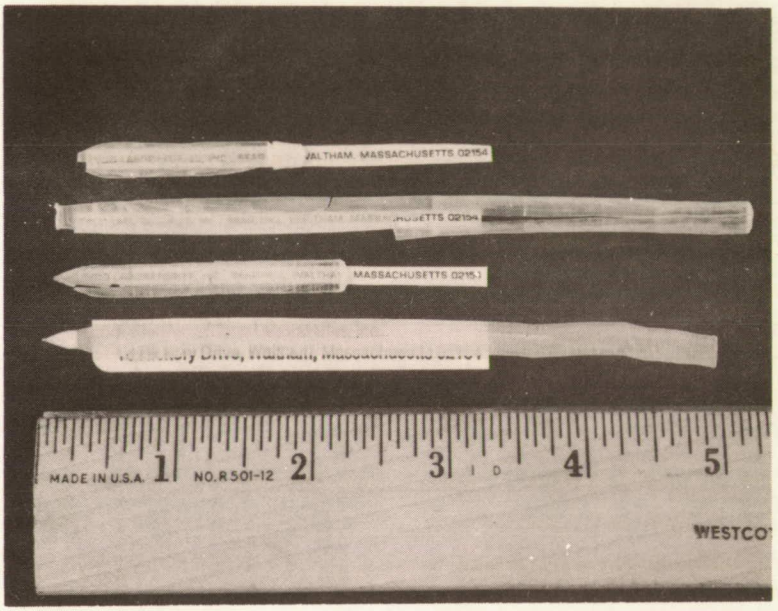

Fig. 19. From top to bottom: Sodium magnesium β " ribbon crystal H.P.-R24 c-axis, H.P.-R25 c-axis, H.P.-R26 a-axis and H.P.-R27 a-axis

Scherrer X-ray spectra of β, β'', β''' and β''''. In Fig. 20 the actual Debye-Scherrer films are compared with a 100% sodium beta-alumina film. As can be seen from these figures the number of phases present increased with crystal length. The phase diagram of Weber and Venero[20] (Fig. 4) does not allow the coexistence of the four phases. That it occurred may be due either to the growth technique which allows segregation to occur at the growth interface or the fact that no part of this is at equilibrium. Two Laue X-ray photographs of the top ribbon face of crystal H.P.-R25 are shown in Fig. 20. This β'' ribbon crystal was seeded in the c-axis direction and Fig. 21a was taken ~6 mm below where it was seeded. As can be seen from Fig. 21b the crystal axis has shifted almost 90° to the a-axis direction after ~2.5 cm of growth. Table V lists the chemical composition of this β'' ribbon crystal. These growth experiments did not yield single phase single crystalline sodium magnesium β'' alumina ribbon crystals.

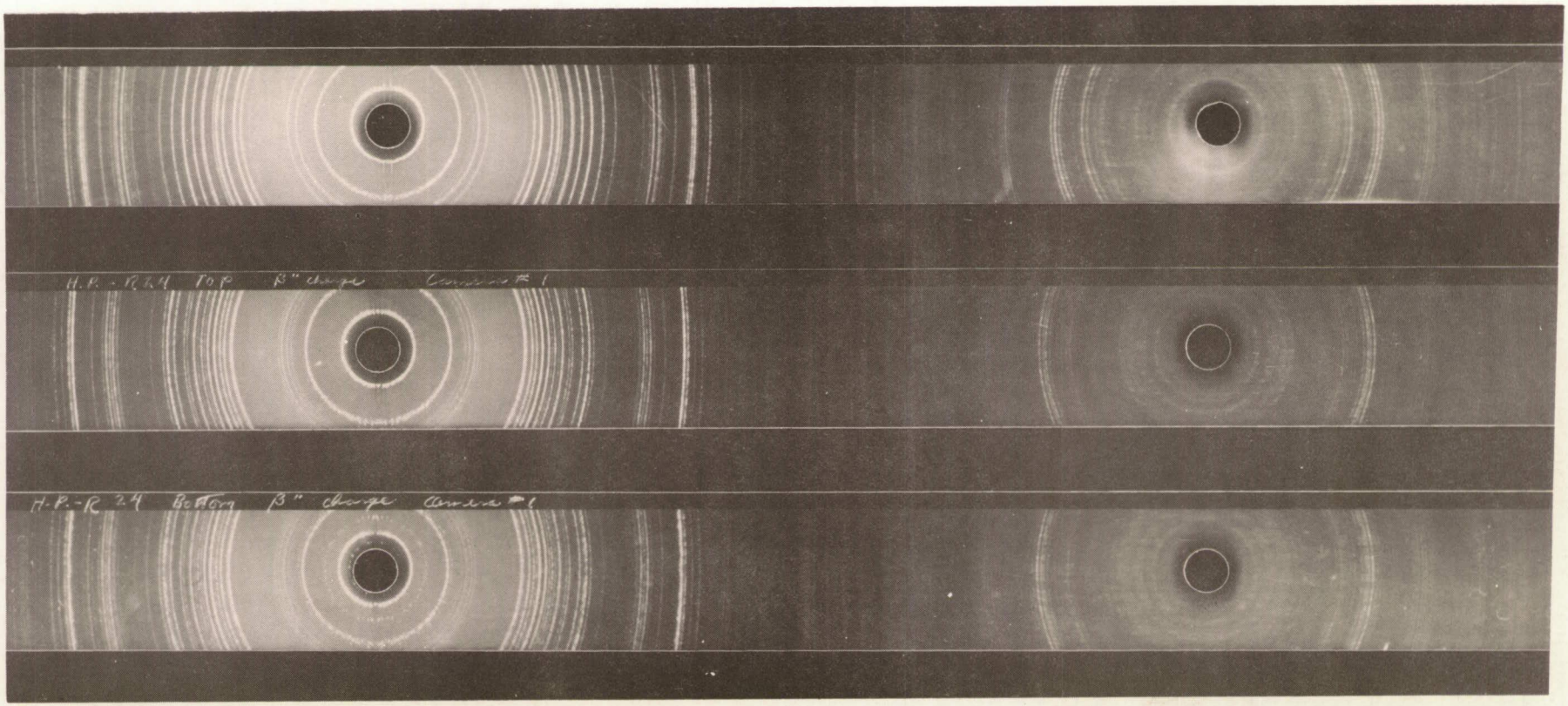

Fig. 20. Compares Debye-Scherrer X-ray film of Monofrax H. Beta-alumina (top film) with Debye-Scherrer X-ray film of top of H.P.-R24 β " (middle film) and Debye-Scherrer X-ray film of bottom of H.P.-R24 β " (bottom film)

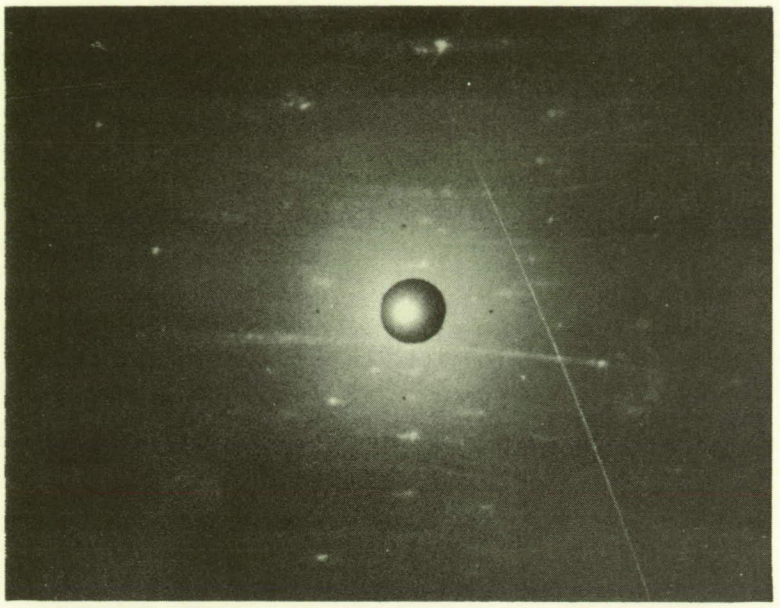

Fig. 21a. Laué X-ray photograph (taken 90° to c-axis) of H.P.-R25 β" c-axis ribbon. Photograph taken of ribbon face just below where it was seeded. Top of ribbon is to the left of the photograph and the ribbon axis goes from left to right

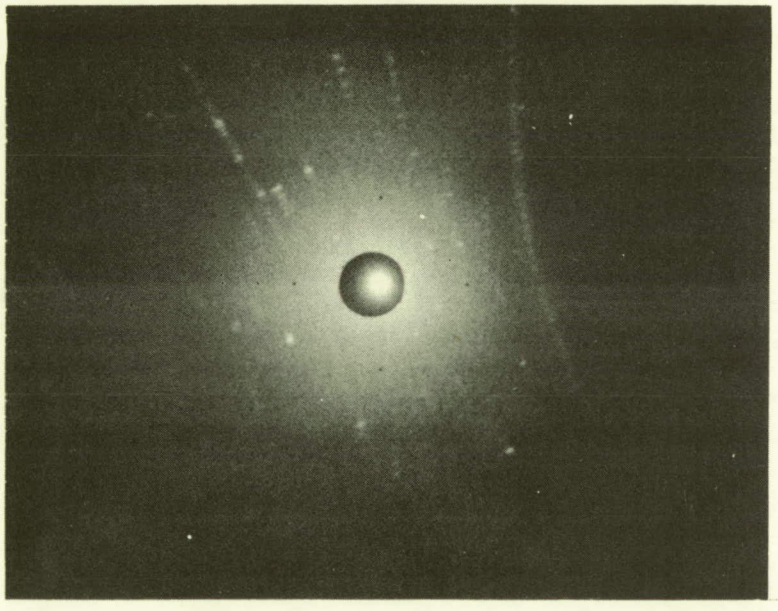

Fig. 21b. Laué X-ray photograph (90° to c-axis) of H.P.-R25 β" c-axis ribbon. Photograph taken ~2.5 cm below top photograph of ribbon face and shows shift of crystal axis of almost 90° from c to a-axis. Top of ribbon is to the left of the photograph, ribbon a-axis goes from left to right

V. CONCLUSIONS

Although single crystal tubes and ribbons of sodium and sodium magnesium beta-alumina and magnesium β'' alumina were grown, the problem of consistently growing useful transparent, uncoated ribbons at speeds > 6 mm/hr remains.

Material grown under this contract has been delivered to NASA-Lewis for ionic conductivity measurements.

VI. REFERENCES

1. N. Weber and J. T. Krummer, Advances in Energy Conversion Engineering, 1967 Intersociety Energy Conversion Engineering Conference, p. 913.
2. J. T. Kummer, Progress in Solid State Chemistry, 7, (1972).
3. M. S. Wittingham and R. A. Huggins, J. of Chem. Phys., 54 (1971).
4. Yung-Fong Yee Sao and J. T. Kummer, J. Inog. Nucl. Chem. 29, 2453 (1967).
5. M. J. Rice and W. L. Roth, J. of Solid State Chem., 4, 294-310 (1972).
6. R. W. Stormont and F. H. Cocks, Final Report, NASA-Lewis Research Center, Contract NAS3-15685, October 1972.
7. J. T. A. Pollock, R. Stormont, and F. Wald, Final Report, NASA-Lewis Research Center, Contract NAS3-14410, June 1971.
8. R. J. Gelsing, et al., Rec. Trav. Chim., 84, 1452 (1965).
9. A. D. Wadsley in "Non-stoichiometric Compounds," L. Mandelcorn (ed.), p. 99, Academic Press, N. Y. (1964).
10. K. Norrish, Min. Mag., 29, 496 (1951).
11. G. Bayer and W. Hoffman, Am. Mineral, 51, 511 (1966).
12. A. Bystrom and A. M. Bystrom, Acta Cryst., 3, 146 (1950).
13. F. H. Cocks and R. W. Stormont, J. Elec. Chem. Soc., 121, Vol. 4 (1974).
14. A. D. Morrison, R. W. Stormont and F. H. Cocks, Am. Cer. Soc., 76th Annual Meeting, Abstract in Am. Cer. Soc. Bull. 53, Vol. 4 (1974).
15. N. Weber and A. F. Venero, Revision of the Phase Diagram $NaAlO_2$ - Al_2O_3, Annual Meeting of Am. Cer. Soc., May 1970
16. Mituo Harata, Mat. Res. Bull., Vol .6, p. 461-464 (1971).

17. A. I. Mlavsky and H. E. LaBelle, Jr., Mat. Res. Bull, 6, 571 (1971).

18. H. E. LaBelle, Jr., Mat. Res. Bull., 6, 581 (1971).

19. R. C. DeVries and W. L. Roth, J. of the Am. Cer. Soc., 52, 364 (1969).

20. N. Weber, and A. F. Venero, Paper 1-JV-70, 72nd Annual Mtg. Am. Cer. Soc., Abstract in Am. Cer. Soc. Bull. 49, 499 (1970).

DISTRIBUTION LIST

NASA

NASA-Lewis Research Center
Attn: A.C. Antoine (M.S. 309-1)
21000 Brookpark Road
Cleveland, OH 44135 (3 copies)

NASA-Lewis Research Center
Attn: L.W. Schopen (M.S. 500-206)
21000 Brookpark Road
Cleveland, OH 44135

NASA-Lewis Research Center
Attn: N.T. Musial (M.S. 500-113)
21000 Brookpark Road
Cleveland, OH 44135

NASA Scientific and Technical Information Facility
Attn: Acquisitions Branch
P. O. Box 33
College Park, MD 20740 (10 copies)

NASA-Lewis Research Center
Attn: Library (M.S. 60-3)
21000 Brookpark Road
Cleveland, OH 44135 (2 copies)

NASA-Lewis Research Center
Attn: Report Control Offices (M.S. 5-5)
21000 Brookpark Road
Cleveland, OH 44135

National Aeronautics and Space Administration
Scientific and Technical Information Facility
P. O. Box 33
College Park, MD 20740
(2 copies and 1 repro)

Mr. Simon Manson, Code ES
National Aeronautics and Space Administration
Washington, DC 20546

Mr. Floyd Ford, Code 761.z
Goddard Space Flight Center
National Aeronautics and Space Administration
Greenbelt, MD 20771

Mr. Gerald Halpert, Code 761.z
Goddard Space Flight Center
National Aeronautics and Space Administration
Greenbelt, MD 20771

Mr. Thomas Hennigan, Code 761
Goddard Space Flight Center
National Aeronautics and Space Administration
Greenbelt, MD 20771

Dr. Louis Rosenblum, (M.S. 302-1)
Lewis Research Center
National Aeronautics and Space Administration
21000 Brookpark Road
Cleveland, OH 44135

Mr. Harvey Schwartz, (M.S. 309-1)
Lewis Research Center
National Aeronautics and Space Administration
21000 Brookpark Road
Cleveland, OH 44135

Dr. J. Stuart Fordyce, (M.S. 309-1)
Lewis Research Center
National Aeronautics and Space Administration
21000 Brookpark Road
Cleveland, OH 44135

Mr. Charles B. Graff, S & E-ASTR-EP
George C. Marshall Space Flt. Center
National Aeronautics and Space Administration
Huntsville, AL 35812

Mr. Hoyt McBryar, EP5
Johnson Space Center
National Aeronautics and Space Administration
Houston, TX 77058

JPL

Mr. Daniel Runkle, (M.S. 198-220)
Jet Propulsion Laboratory
4800 Oak Grove Drive
Pasadena, CA 91103

Dr. R. Lutwack, (M.S. 198-220)
Jet Propulsion Laboratory
4800 Oak Grove Drive
Pasadena, CA 91103

Mr. Aiji A. Uchiyama, (M.S. 198-220)
Jet Propulsion Laboratory
4800 Oak Grove Drive
Pasadena, CA 91103

ARMY

Harry Diamond Laboratories
Room 300, Bldg. 92
Connecticut Ave. & Van Ness St., N.W.
Washington, DC 20438

U. S. Army Electronics Command
Attn: AMSEL-TL-P
Fort Monmouth, NJ 07703

Commanding Officer
U. S. Army Mobility Equip. Research & Development Center
Electrotechnology Department
Electrochemical Division
Attn: SMEFB-EE
Fort Belvoir, VA 22061

NAVY

Director, Power Program, Code 473
Office of Naval Research
Arlington, VA 22217

Dr. George A. Neece, Code 472
800 N. Quincy St.
Office of Naval Research
Arlington, VA 22217

Mr. S. Schuldiner, Code 6160
Naval Research Laboratory
4555 Overlook Avenue, S.W.
Washington, DC 20375

Mr. J. H. Harrison, Code 2724
Naval Ship R & D Center
Annapolis, MD 21402

Commanding Officer
Naval Ammunition Depot
(305, Mr. D. G. Miley)
Crane, IN 47522

Mr. Phillip B. Cole, Code 232
Naval Ordnance Laboratory
Silver Spring, MD 20910

Mr. Albert Himy, 6157D
Naval Ship Engineering Center
Center Bldg., Prince Georges Center
Hyattsville, MD 20782

Dr. H. E. Ruskie, NISC-4321
4301 Suitland Road
Suitland, MD 20390

Arthur M. Diness, Code 471
Office of Naval Research
Arlington, VA 22217

AIR FORCE

AFAPL/POE-1/D. R. Warnock
Wright-Patterson AFB, OH 45433

Air Force Aero Propulsion Lab.
POE-1/W. S. Bishop
WPAFB, OH 45433

Mr. Edward Raskind, LCC, Wing F
U. S. AF Cambridge Research Lab.
L. G. Hanscom Field
Bedford, MA 01731

Rome Air Development Center
Attn: TUGG/F. J. Mollura
Griffiss AFB, NY 13441

SAMSO/DYAE
P. O. Box 92960
Worldway Postal Center
Los Angeles, CA 90009

OTHER GOVERNMENT ORGANIZATION

Dr. Leonard Topper
NSF, RANN
Washington, DC 20550

PRIVATE ORGANIZATIONS

Dr. E. A. Heintz
Technical Department
Airco Speer Carbon-Graphite
P. O. Box 828
Niagara Falls, NY 14302

Dr. R. T. Foley
Chemistry Department
American University
Massachusetts & Nebraska Aves., N.W.
Washington, DC 20016

Mr. R. A. Knight
Research Division
AMF Inc.
689 Hope Street
Stamford, CT 06907

Dr. H. Shalit
ARCO Chemical Co.
Div. of Atlantic Richfield Co.
500 South Ridgeway Avenue
Glenolden, PA 19036

Dr. James D. Birkett
Arthur D. Little, Inc.
Acorn Park
Cambridge, MA 02140

Dr. H. L. Recht
Atomics International Division
International Corp.
P. O. Box 309
Canoga Park, CA 91304

Mr. R. F. Fogle, GA 28
North American Rockwell
Autonetics Division, NAR
P. O. Box 4192
Anaheim, CA 92803

Mr. J. E. Clifford, Technical Representative
Electrochemical Eng. Technical Div.
Battelle
Columbus Laboratories
505 King Avenue
Columbus, OH 43201

Mr. D. O. Feder
Bell Telephone Laboratories, Inc.
Murray Hill, NJ 07974

Dr. Carl Berger
13401 Kootenay Drive
Santa Ana, CA 92705

Mr. Sidney Gross, (M.S. 8E-37)
The Boeing Company
P. O. Box 3999
Seattle, WA 98124

Professor T. P. Dirkse
Calvin College
3175 Burton Street, S.E.
Grand Rapids, MI 49506

Prof. Ernest Yeager
Department of Chemistry
Case Western Reserve Univ.
Cleveland, OH 44106

Mr. C. E. Thomas
Chrysler Corporation
Space Division
Dept. 2730
P. O. Box 29200
New Orleans, LA 70189

Mr. E. P. Broglio
Eagle-Picher Industries, Inc.
P. O. Box 47, Couples Dept.
Joplin, MO 64801

Dr. J. M. Williams
Experimental Station, Bldg. 304
Engineering Technology Lab.
E. I. duPont de Nemours & Co.
Wilmington, DE 19898

Mr. R. P. Mikkelson
Electrical Systems Dept. 623-2
General Dynamics/Convair Aerospace Division
P. O. Box 80847
San Diego, CA 92138

Xerox Corporation
Electro-Optical Systems
800 North Halstead Street
Pasadena, CA 91107

Mr. Martin Klein
Energy Research Corporation
15 Durant Avenue
Bethel, CT 06801

Dr. J. G. Cohn
Engelhard Industries
Menlo Park
Edison, NJ 08817

Mr. L. Berkowitz
Government Research Lab.
Esso Research and Engineering Co.
P. O. Box 8
Linden, NJ 07036

Dr. Arthur Fleischer
466 South Center Street
Orange, NJ 07050

The Garrett Corporation
Suite 515, Cafritz Building
1625 Eye Street, N.W.
Washington, DC 20006

Dr. J. B. Bush, Jr.
Research and Development Center
General Electric Company
Bldg. K-1 Rm. 4A28
P. O. Box 8
Schenectady, NY 12301

Mr. Kenneth Hanson
General Electric Company
Valley Forge Space Technology Center
P. O. Box 8555
Philadelphia, PA 19101

Mr. J. A. Keralla
Delco Remy Division
General Motors Corporation
2401 Columbus Avenue
Anderson, IN 46011

Dr. John McCallum,
President
Invention Talents, Inc.
1149 Chesepeake Avenue
Columbus, OH 43212

Mr. L. J. Nuttall
General Electric Company
930 Western Avenue, 274A4
Lynn, MA 01910

Mr. F. T. O'Brien
Direct Energy Conversion Programs
General Electric Company
930 Western Avenue
Lynn, MA 01910

Dr. E. L Simons
Environmental Protection Operation - Bldg. 36
General Electric Company
Schenectady, NY 12345

Dr. G. Goodman
Globe-Union, Inc.
P. O. Box 591
Milwaukee, WI 53201

Dr. J. E. Oxley
Dr. B. B. Owens
Gould Inc., Gould Lab.
P. O. Box 3140
St. Paul, MN 55165

Grumman Aerospace Corp.
S. J. Gaston, Plant 35,
Dept. 553
Bethpage, Long Island, NY 11714

Gulton Battery Corporation
212 Durham Ave.,
Middlesex County
Metuchen, NJ 08840

Dr. P. L. Howard
Millington, MD 21651

Dr. M. E. Ellion, Manager
Propulsion & Power Systems Lab.
Bldg. 366, MS 524
Hughes Aircraft Company
El Segundo, CA 90245

Mr. R. Hamilton
Institute for Defense Analyses
400 Army-Navy Drive
Arlington, VA 22202

Mr. James R. Hunt
International Nickel Company
1000-16th Street, N.W.
Washington, DC 20036

Dr. A Moos
Leesona Corporation
Warwick, RI 02887

Dr. R. A. Wynveen, President
Life Systems, Inc.
23715 Mercantile Road
Cleveland, OH 44122

Mr. Robert E. Corbett
Department 62-25, Bldg. 151/1
Lockheed Aircraft Corporation
P. O. Box 504
Sunnyvale, CA 94088

Mr. S. J. Angelovich
Chief Engineer
Mallory Battery Company
South Broadway
Tarrytown, NY 10591

Mr. A. D. Tonelli
Dept. A3-833, MS 22-2
McDonnell Douglas Astronautics Co.
5301 Bolsa Avenue
Huntington,Beach, CA 92647

Dr. Robert C. Shair
4921 Sanayer Drive
Hollywood, FL 33021

Rocketdyne Division
North American Rockwell Corp.
Attn: Library
6633 Canoga Avenue
Canoga Park, CA 91304

National Center for Energy Management & Power
113 Towne Building
University of Pennsylvania
Philadelphia, PA 19104

Dr. C. Bocciarelli
112 E 2nd Street
Moorestown, NJ 08057

Mr. D. C. Briggs
WDL Division
Philco-Ford Corporation
3939 Fabian Way
Palo Alto, CA 94303

Dr. Per Bro
P. R. Mallory & Company, Inc.
Northwest Industrial Park
Third Avenue
Burlington, MA 01801

P. R. Mallory & Company, Inc.
Library
P. O. Box 706
Indianapolis, IN 46206

Mr. V. D'Agostino
RAI Research Corporation
225 Marcus Blvd.
Hauppauge, LI, NY 11787

Southwest Research Institute
Attn: Library
P. O. Drawer 28510
San Antonio, TX 78284

Library
Sanford Research Institute
333 Ravenswood Avenue
Menlo Park, CA 94025

Dr. W. R. Scott (M1-1208)
TRW Systems, Inc.
One Space Park
Redondo Beach, CA 90278

Dr. Herbert P. Silverman
(R-1/2094)
TRW Systems, Inc.
One Space Park
Redondo Beach, CA 90278

Union Carbide Corporation
Battery Products Division
Development Laboratory Library
P. O. Box 6056
Cleveland, OH 44101

Dr. Robert Powers
Consumer Products Division
Union Carbide Corporation
P. O. Box 6116
Cleveland, OH 44010

United Aircraft Corporation
Attn: Library
400 Main Street
East Hartford, CT 06108

Power Information Center
University City Science Institute
3401 Market Street, RM 2210
Philadelphia, PA 19104

Dr. Frederick Morse
Dept. of Mechanical Engineering
University of Maryland
College Park, MD 20742

Yardney Electric Corporation
Power Sources Division
3850 Olive Street
Denver, CO 80207

Yardney Electric Division
82 Mechanic Street
Pawcatuck, CT 02891

Dr. Eugene Y. Weissman, Director
Inorganic-Electrolytic R & D
BASF Wyandotte Corporation
Wyandotte, MI 48192

Dr. Charles Levine
Dow Chemical U.S.A.
Walnut Creek Research Center
2800 Mitchell Drive
Walnut Creek, CA 94598

Prof. Donald M. Smyth
Materials Research Center
Lehigh University
Bethlehem, PA 18015

Prof. John W. Patterson
Dept. of Metallurgy
Iowa State University
Ames, IA 50010

Prof. Rustum Roy
Materials Science Dept.
Pennsylvania State University
University Park, PA 16802

Prof. John H. Kennedy
Univ. of Calif. at Santa Barbara
Santa Barbara, CA 93106

Dr. Paul Jorgensen
Stanford Research Institute
Menlo Park, CA 94025

Dr. L. Topper
Div. of Advanced Technology Applications
National Science Foundation
Washington, DC 20550

Mr. L. R. Rothrock
Union Carbide Corp.
8888 Balboa Avenue
San Diego, CA 92123

Prof. K. E. Cox
Dept. of Chem. & Nucl. Eng.
Tech. Appl. Center
University of New Mexico
Albuquerque, NM 87131

Dr. Robert A. Huggins
Dept. of Materials Science and Engineering
Stanford University
Stanford, CA 94305

Dr. M. Stanley Whittingham
Esso Research and Engineering Co.
Linden, NJ 07036

Dr. Neill T. Weber
Ford Motor Co. Research Lab
Dearborn, MI 48121

Prof. James L Mueller
Ceramic Engineering Div.
University of Washington
Seattle, WA 98195

Dr. Douglas O. Raleigh
North American Rockwell
Science Center
Thousand Oaks, CA 91360

Dr. R. H. Doremus
Rensselaer Polytechnic Institute
Materials Division
Troy, NY 12181

Dr. Robert S. Roth
National Bureau of Commerse
Washington, DC 20234

Prof. Alexander F. Wells
Dept. of Chemistry
University of Connecticut
Storrs, CT 06268

Dr. Elton J. Cairns
Electrochemistry Dept.
General Motors Research Lab
12 Mile and Mound Roads
Warren, MI 48090

Dr. John B. Goodenough
Massachusetts Institute of Technology
Lincoln Laboratory
Lexington, MA 02173